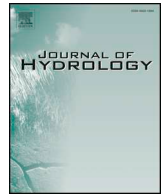




ELSEVIER

Contents lists available at ScienceDirect

Journal of Hydrology

journal homepage: www.elsevier.com/locate/jhydrol

Research papers

An in-situ data based model to downscale radiometric satellite soil moisture products in the Upper Hunter Region of NSW, Australia

I.P. Senanayake^a, I.-Y. Yeo^{a,b,*}, N. Tangdamrongsub^{c,d}, G.R. Willgoose^a, G.R. Hancock^e, T. Wells^a, B. Fang^f, V. Lakshmi^f, J.P. Walker^g^a School of Engineering, Faculty of Engineering and Built Environment, The University of Newcastle, Callaghan, NSW 2308, Australia^b Department of Geographical Sciences, University of Maryland, College Park, MD 20742, USA^c Earth System Science Interdisciplinary Center, University of Maryland, College Park, MD 20740, USA^d Hydrological Sciences Laboratory, NASA Goddard Space Flight Center, Greenbelt, MD 20771, USA^e School of Environmental and Life Sciences, Faculty of Science, The University of Newcastle, Callaghan, NSW 2308, Australia^f Department of Engineering Systems and Environment, University of Virginia, Charlottesville, VA 22904, USA^g Department of Civil Engineering, Monash University, Clayton, Victoria 3800, Australia

ARTICLE INFO

This manuscript was handled with the assistance of Emmanouil Anagnostou, Associate Editor

Keywords:

Downscaling
Disaggregation
Soil moisture
SMAP
SMOS
MODIS

ABSTRACT

High spatial resolution soil moisture information is important for hydrological, climatic and agricultural applications. The lack of high resolution soil moisture data over large areas at the required accuracy is a major impediment for such applications. This study investigates the feasibility of downscaling satellite soil moisture products to 1 km resolution. This study was undertaken in the semi-arid Goulburn River Catchment, located in south-eastern Australia. The Soil Moisture Active Passive (SMAP)-Enhanced 9 km (L3SMP-E) and Soil Moisture and Ocean Salinity (SMOS) 25 km gridded (SMOS CATDS L3 SM 3-DAY) radiometric products were compared with in-situ soil moisture observations and a regression tree model was developed for downscaling based on thermal inertia theory. Observations from a long-term soil moisture monitoring network were employed to develop a regression tree model between the diurnal temperature difference and the daily mean soil moisture for soils with different clay content and vegetation greenness. Moderate-resolution Imaging Spectroradiometer (MODIS) land surface temperatures were used to estimate the soil moisture at high spatial resolution by disaggregating the satellite soil moisture products through the regression model. The downscaled SMAP-Enhanced 9 km and SMOS 25 km gridded soil moisture products showed unbiased root mean square errors (ubRMSE) of 0.07 and 0.05 cm³/cm³, respectively, against the in-situ data. These ubRMSEs include errors caused by measuring instrument and the scale mismatch between downscaled products and in-situ data. An RMSE of 0.07 cm³/cm³ was observed when comparing the downscaled soil moisture against the passive airborne L-band retrievals. The findings here auger well for the use of satellite remote sensing for the assessment of high resolution soil moisture.

1. Introduction

Soil moisture is a key variable in a number of environmental processes at both regional and global scales including hydrologic, climatic and agricultural applications, such as water management and irrigation scheduling (Hanson et al., 2000; Pacheco et al., 2015), weather and climatic prediction (Dirmeyer et al., 2016; Huszar et al., 1999; Orth and Seneviratne, 2014), drought monitoring (Lorenz et al., 2017; Pablos et al., 2017; Wang et al., 2011), flood forecasting (Brocca et al., 2017; Lacava et al., 2005; Norbiato et al., 2008; Trambly et al., 2010) and analysing nutrient and contaminant transport potential (Dickinson

et al., 2002; Porporato and Rodriguez-Iturbe, 2002). Many of these applications require soil moisture data at high spatial resolution, from a few kilometres to sub-kilometre scale. However, soil moisture information is rarely available at adequate spatial and temporal scales. Soil moisture is measured at scales ranging from point (in-situ measurements) to satellite measurements at ~10 s of km scale. Given the limited availability of dense ground-based soil moisture monitoring networks in most areas, satellite soil moisture products are considered a most feasible option to provide spatial and temporal soil moisture data.

Microwave remote sensing has been widely used to estimate global scale surface soil moisture over the last three decades (Karthikeyan

* Corresponding author at: School of Engineering, Faculty of Engineering and Built Environment, The University of Newcastle, Callaghan, NSW 2308, Australia.
E-mail address: In-Young.Yeo@newcastle.edu.au (I.-Y. Yeo).

<https://doi.org/10.1016/j.jhydrol.2019.03.014>

Received 15 May 2018; Received in revised form 4 March 2019; Accepted 11 March 2019

Available online 13 March 2019

0022-1694/ © 2019 Elsevier B.V. All rights reserved.

et al., 2017a; Kerr et al., 2016; Schmugge and Jackson, 1993; Schmugge, 1976). In particular, passive microwave radiometer measurements in the L-band frequency regime have been shown to be the best option to retrieve soil moisture (Schmugge et al., 1986). Recently, satellite soil moisture retrieval from L-band sensors has been realized with the launch of the European Space Agency's (ESA) SMOS (Soil Moisture and Ocean Salinity) and the National Aeronautics and Space Administration's (NASA) Soil Moisture Active Passive (SMAP) satellites in 2009 and 2015, respectively. These satellites provide global estimates of surface soil moisture at the top ~5 cm of the soil profile (Entekhabi et al., 2010a; Karthikeyan et al., 2017b; Kerr et al., 2010) frequently (~3-day revisit period) at an expected accuracy of 0.04 v/v, but with low spatial resolution (~40 km). SMAP employs vertically polarized brightness temperature-based single-channel algorithm (SCAV) as the current baseline retrieval algorithm for its passive soil moisture product (Chan et al., 2018). The L-band Microwave Emission of the Biosphere Model (L-MEB) is currently used as the retrieval algorithm for the SMOS products (Kerr et al., 2012; Wigneron et al., 2007). Despite their high accuracy, the satellite products cannot fully capture the spatial variability of soil moisture as required in many applications, due to their coarse resolutions.

Validating and downscaling satellite soil moisture products are crucial for their utilization in various applications. For example, extensive calibration and validation (cal/val) activities pre- and post-launch of SMAP have been used to develop and improve the retrieval algorithms using in-situ soil network measurements (Jackson et al., 2014). The quality requirement of in-situ data, and the spatial mismatching between remotely sensed and in-situ soil moisture, posed great challenges for the validation of satellite soil moisture products (Colliander et al., 2017a; Crow et al., 2012; Jackson et al., 2014). The intensive cal/val phase of the SMAP mission demonstrated the SMAP radiometer based soil moisture products meet their expected performance (~0.04 m³/m³) from globally selected core validation sites (Colliander et al., 2017a).

Given the accuracy of passive L-band microwave remote sensing, downscaling these reliable satellite soil moisture products is a logical step to estimate soil moisture at the required spatial resolution for many applications (Peng et al., 2017; Sabaghy et al., 2018). The available satellite soil moisture downscaling methods can be classified as; satellite, geo-information data, and model based approaches (Peng et al., 2017). Satellite based soil moisture downscaling methods consist of fusion of active and passive microwave retrievals (Das et al., 2011, 2014, 2018; Leroux et al., 2016) and fusion of microwave data with optical or thermal datasets (Piles et al., 2014, 2016, 2011; Portal et al., 2018; Sánchez-Ruiz et al., 2014; Chauhan et al., 2003). The downscaled soil moisture of the active passive microwave data fusion methods provides products with a moderate resolution. Since Carlson et al. (1994) introduced the 'universal triangle' concept between soil moisture, surface temperature and vegetation index, efforts have been made to downscale satellite soil moisture products by introducing optical/thermal data. Optical/thermal based downscaling approaches provide higher resolution soil moisture products and perform well in arid and semi-arid areas with high atmospheric evaporative demand (Peng et al., 2017). Therefore, these methods have a high potential over the Australian land mass in developing a time series record of high resolution soil moisture. In these approaches, land surface parameters (e.g., vegetation cover, land surface temperature, surface albedo) retrieved from the optical/thermal satellite sensors at a high spatial resolution, have been expressed as a function of soil moisture (Carlson, 2007; Chauhan et al., 2003; Merlin et al., 2010, 2012; Peng et al., 2017; Petropoulos et al., 2009; Piles et al., 2011). The Disaggregation based on Physical And Theoretical scale Change (DisPATCH) model proposed by Merlin et al. (2012) is one such method of downscaling microwave soil moisture retrievals using optical/thermal data. In this study, MODerate-resolution Imaging Spectroradiometer (MODIS) products were used to derive land surface temperatures (LSTs) at high spatial

resolution (1 km). The MODIS-derived LSTs were separated into their soil and vegetation components as in the 'universal triangle' or 'trapezoidal model'. The soil evaporative efficiency (SEE) (estimated using MODIS LSTs), albedo, and Normalized Difference Vegetation Index (NDVI) were related to the soil moisture variability within a coarse resolution SMOS pixel (Merlin et al., 2008, 2010, 2012). The accuracy of the downscaled products from DisPATCH showed a notable variation with the season, showing root mean square errors (RMSEs) of 0.06 m³/m³ in Austral summer and 0.18 m³/m³ in Austral winter when compared with the in-situ soil moisture, in the Murrumbidgee River catchment (Merlin et al., 2012; Sabaghy et al., 2018).

Fang et al. (2013) and Fang and Lakshmi (2014) proposed a regression model to downscale the SMOS and the Advanced Microwave Scanning Radiometer for the Earth Observing System (AMSR-E) soil moisture products. This downscaling approach is based on the thermal inertia relationship between the diurnal soil temperature difference (ΔT) and the daily mean soil moisture ($\theta\mu$). Model derived soil moisture and soil temperature estimates from North American Land Data Assimilation System (NLDAS), NDVI data from MODIS, Satellite Pour l'Observation de la Terre (SPOT) and Advanced Very High Resolution Radiometer (AVHRR) along with the MODIS LST products were used to demonstrate the capability of the proposed downscaling model over Oklahoma, Midwest region of the United States. The downscaled soil moisture showed RMSEs ranging from 0.02 to 0.06 m³/m³ over the Little Washita Watershed in Oklahoma (Fang and Lakshmi, 2014), and unbiased RMSEs (ubRMSE) of 0.042 m³/m³ and 0.026 m³/m³ against ground observations from the soil monitoring networks (Fang et al., 2013). The spatial data gaps due to cloud cover and impact of vegetation on optical/thermal observations are two major limitations in the optical/thermal data based downscaling methods (Peng et al., 2017; Sabaghy et al., 2018).

The study presented in this paper investigates the feasibility of developing a time series record of high spatial resolution soil moisture by downscaling satellite soil moisture products using an in-situ data based model. The regression tree method developed here is similar to Fang et al. (2013, 2018) and Fang and Lakshmi (2014), but based on in-situ observations with additional factors. Fang et al. (2013) and Fang and Lakshmi (2014) developed monthly lookup regressions using model derived ΔT and $\theta\mu$ modulated by the NDVI, and then used this regression tree method to downscale AMSR-E and SMOS soil moisture products using MODIS LSTs. Since global scale land surface models are not fully calibrated to specific sites, these products can be associated with high uncertainties caused by scaling issues, accuracy of the input data and the model-algorithms (Chen et al., 2014). For arid or semi-arid landscapes with the extreme climate variability and the complex ecosystem, global land surface modelled data can be subjected to high prediction errors and they may not be reliable reference data for representing actual soil conditions without rigorous calibration and validation. To avoid the uncertainties and errors associated with the model-derived estimates, the study presented here employed a high quality, reliable in-situ observations of soil moisture and temperature over a long period from well-designed and maintained monitoring sites (described in Section 2.2.1) to develop the downscaling model. Also, the downscaling model was generalized over the study catchment area, i.e., relative soil moisture variability to mean catchment soil moisture condition, considering site-specific soil characteristics as a modulating factor to explain the spatial variability and temporal stability of surface soil moisture in a semi-arid region (Cosh et al., 2008; Chen et al., 2014).

As the first step, SMAP-Enhanced 9 km and SMOS 25 km gridded soil moisture products were compared with in-situ soil moisture observations and then a regression tree model was developed to downscale the satellite soil moisture products to 1 km resolution based on thermal inertia theory. Finally, the reliability of the downscaled products was assessed using ground observations and an airborne soil moisture retrieval. The study presented in this paper was undertaken in the Goulburn River Catchment, located in the south-eastern region of

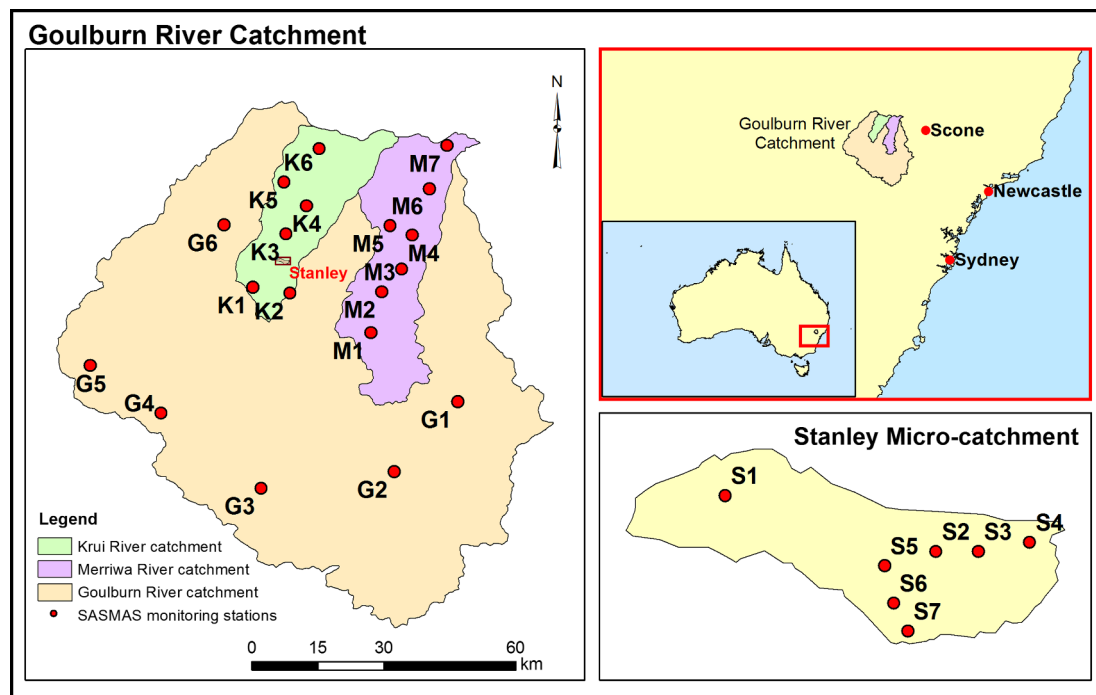


Fig. 1. The location of the Goulburn River catchment, and the distribution of the monitoring stations established under the SASMAS project.

Australia, where significant efforts have been made to measure soil moisture through continuous in-situ soil moisture monitoring network, field-based studies, and remote sensing (Chen et al., 2014; Martínez et al., 2007; Panciera et al., 2008; Rüdiger et al., 2007).

2. Study area and data

2.1. Description of the study area

The Goulburn River catchment is located approximately 150 km northwest of Sydney, extending from 31°46'S to 32°51'S and from 149°40'E to 150°36'E (Fig. 1). The Goulburn River is a tributary of the Hunter River in south-eastern Australia. The catchment size is ~7000 km² and its elevation varies from 100 m on the floodplains to 1300 m in the northern and southern mountain ranges. The northern and southern halves of the catchment can be distinguished both geologically and on the basis of land use/land cover. The northern half of the catchment is dominated with basalt derived soils while the southern part is dominated with sandstone, conglomerate and shale derived soils. The northern part has been cleared mainly for cropping and grazing, whereas the southern part consists of dense vegetation with forests. The distribution of clay, silt and sand contents of the top soils in the catchment is shown in Fig. 2. The area exhibits a semi-arid climate with a mean annual precipitation of 700 mm. However, the study catchment shows an increasing gradient in precipitation towards higher altitudes resulting in a range from 500 mm to 1100 mm. The monthly mean temperatures vary from 16 °C to 30 °C in the summer and from 3 °C to 17 °C in the winter (Rüdiger et al., 2003). This region has experienced a range of climatic events during the last 15 years, including the millennium drought from 2001 to 2009 (Van Dijk et al., 2013), strong La Niña conditions in 2010/11 (Boening et al., 2012) and an extreme storm event with a 100-year return period (Pasha Bulker storm) in 2007 (Mills et al., 2010).

The study site has been thoroughly studied in order to develop a better understanding of the land surface processes driving soil moisture variability. Under the Scaling and Assimilation of Soil Moisture and Streamflow (SASMAS) project, the study site has been heavily instrumented for soil moisture, rainfall, and runoff since 2002 (Rüdiger

et al., 2007). The monitoring stations were established to provide in-situ data to validate AMSR-E soil moisture retrievals, develop down-scaling algorithms for coarse resolution satellite soil moisture products, assimilate remotely sensed soil moisture data to retrieve soil moisture profile and to improve streamflow forecasting (Rüdiger et al., 2003). National Airborne Field Experiment 2005 (NAFE'05) airborne campaign was conducted in this area using L-band radiometers to provide simulated SMOS observations for soil moisture while validating the AMSR-E near-surface soil moisture products (Panciera et al., 2008).

This study is focused on two sub-catchments, the Krui (562 km²) and Merriwa (651 km²) River, located in the northern half of the Goulburn River catchment. These sub-catchments include a dense soil moisture monitoring network (Fig. 1) and have been mostly cleared for cropping and grazing (Fig. 3a). Fig. 3b shows the average seasonal vegetation density in 2015 as inferred by the MODIS NDVI composites over these two sub-catchments. The dense vegetation in the north and south-most parts of the two sub-catchments is evident in Fig. 3b. The temporal dynamics of NDVI in the Krui River catchment SASMAS monitoring stations retrieved from the MODIS 16-day NDVI composites are shown in Fig. 4. A high variability of NDVI can be observed at stations in croplands (i.e. K1 and K3), compared to the other stations which are in grazing areas. K6 shows a consistently high NDVI value, possibly due to the high vegetation growth driven by the higher rainfall.

2.2. Data

This section discusses details on in-situ soil moisture observations, the satellite soil moisture products, and other geospatial data used for developing the downscaling algorithm. Table 1 provides a summary of the datasets used in this study.

2.2.1. In-situ soil moisture observations

Twenty-six soil moisture and temperature monitoring stations were established from 2002 over the Goulburn River catchment under the SASMAS project (<http://www.eng.newcastle.edu.au/sasmas/SASMAS/sasmas.htm>). The SASMAS soil moisture monitoring stations were established in the representative, 'time stable' locations of their

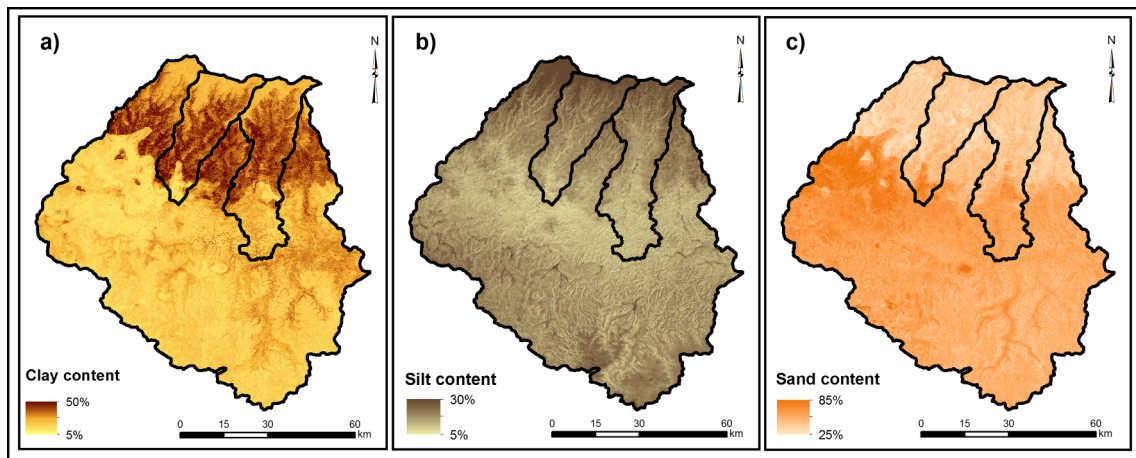


Fig. 2. Soil (a) clay, (b) silt, and (c) sand contents of the top 5 cm soil profile in the Goulburn River catchment (Source: National Soil and Landscape Grid, Australia).

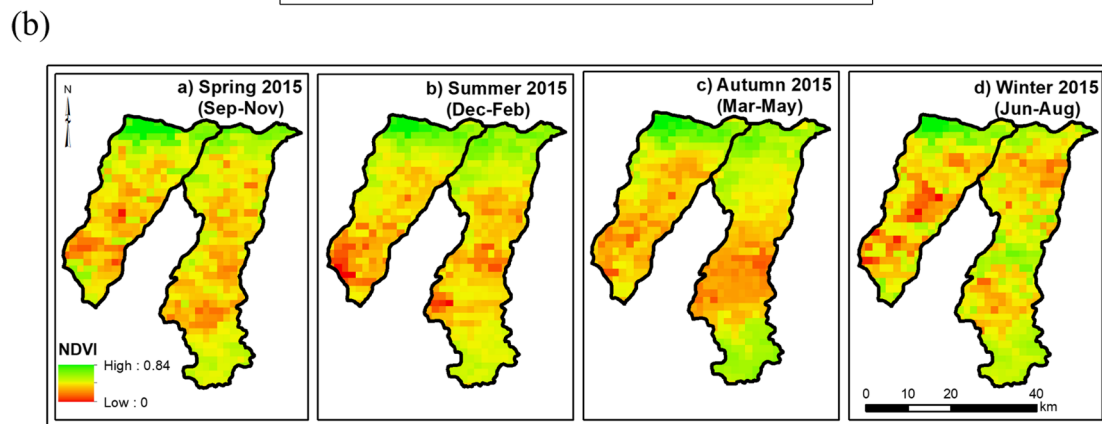
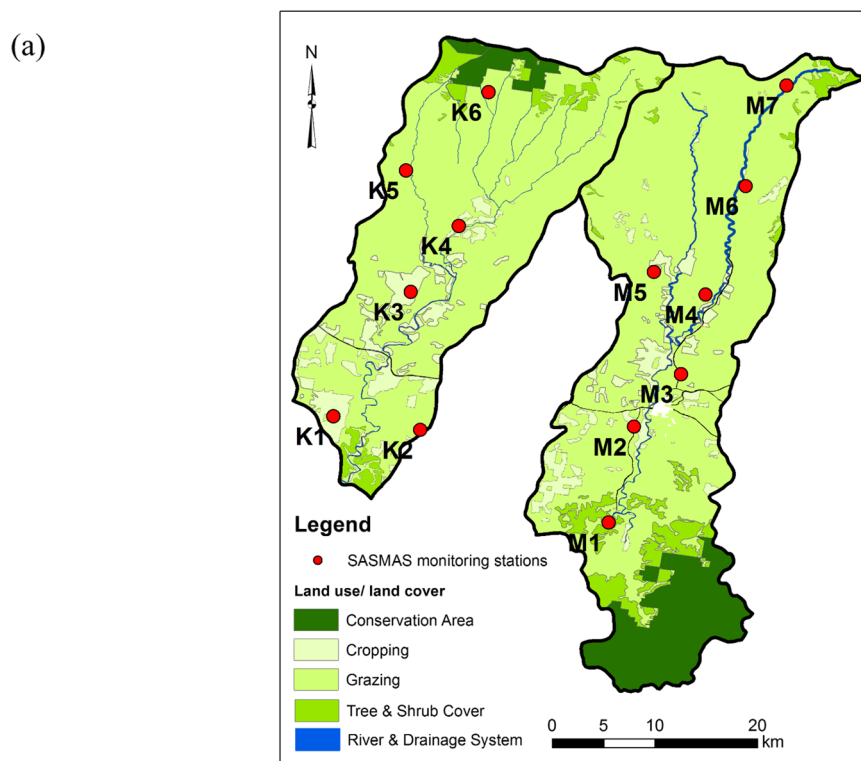


Fig. 3. (a) Land use/land cover of Krui and Merriwa River catchments. (Source: The Department of Environment and Climate Change, NSW). (b) Seasonal average NDVI maps in 2015 of Krui and Merriwa River catchments calculated by using MODIS 16-day NDVI composites.

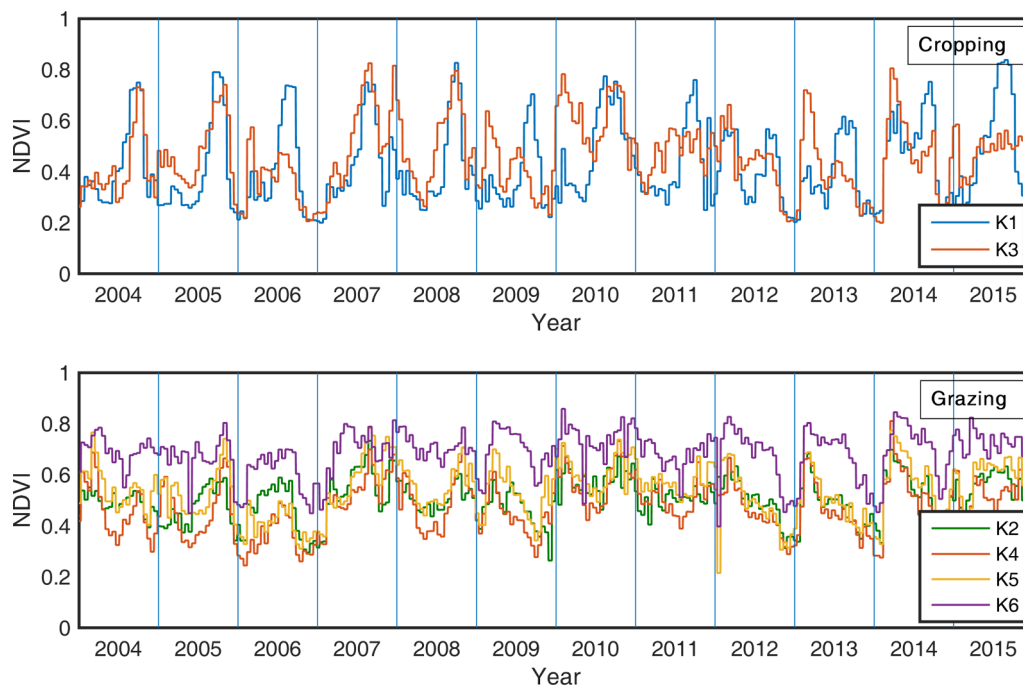


Fig. 4. The temporal variability of vegetation in Krui River catchment SASMAS monitoring stations as captured by the MODIS 16-day NDVI composites (MYD13A2).

surrounding landscape, so that they could adequately represent the watershed as whole and the footprint scale radiometric satellite soil moisture products after upscaling (Grayson and Western, 1998; Rüdiger et al., 2003, 2007; Crow et al., 2012). These sites were carefully chosen by selecting mid-slope locations with representative vegetation, soil type, elevation, aspect, etc. (Rüdiger et al., 2003, 2007). During the NAFE'05, an intensive field campaign had been carried out to support the L-band airborne soil moisture observations. This ground sampling had been conducted from very high resolutions (6.25 and 12.5 m spacing) to intermediate resolutions from 125 m to 250 m spacing and coarse resolutions from 500 m and/or 1 km spacing. The NAFE'05 data analysis showed the potential of using the SASMAS dataset to validate coarse resolution satellite soil moisture products such as SMOS over the Goulburn River catchment area (Panciera et al., 2008). The sites have been instrumented with three vertically inserted Campbell Scientific CS616 water content reflectometers at soil depths of 0–30, 30–60 and 60–90 cm, at each station. Stevens Water HydraProbes were later installed to measure soil temperature at 25 mm and soil moisture of the top 5 cm soil layer at the monitoring stations (Rüdiger et al., 2007). Six monitoring stations were established in the Krui River catchment (K1 to K6) and seven in the Merriwa River catchment (M1 to M7). In addition, seven monitoring stations (S1 to S7) were established over a densely monitored micro-catchment, “Stanley” (with a catchment size of 175 ha) located within the Krui River catchment (Martinez et al., 2007) (Fig. 1). These monitoring stations are located over a range of soil types, varying from sandy to clayey soils. The land cover and soil texture of the SASMAS stations in the Krui and Merriwa River catchments are shown in Table 2. The in-situ soil moisture data were measured at 1 min interval and averaged using 20 min time window. The SASMAS dataset is available from 2003 to 2015, but contains a number of data gaps. These data gaps are caused mainly due to failure of sensors/telemetry, and erroneous readings caused by extremely dry weather conditions that resulted in soil cracking, especially dominate in the clay soils in the northern parts of the sub-catchments. Erroneous readings were recorded at some of the stations during this time due to sensors not remaining in contact with soils during dry periods and the cracks getting filled with water during wet periods. The SASMAS datasets are available up to 2015. The daily mean soil moisture data and hourly soil temperature data of the 0–5 cm soil profile from 2003 to 2014 were

employed in this study to develop the regression algorithms. The daily mean soil moisture data in 2015 from the Krui, Merriwa and Stanley stations were employed in the validation of satellite and downscaled soil moisture products (details discussed in Section 3).

2.2.2. Satellite soil moisture products

The ESA's SMOS mission launched in 2009 (Barré et al., 2008; Kerr et al., 2010) and the NASA's SMAP launched in 2015 (Chan et al., 2016; Entekhabi et al., 2010a) are two L-band missions which use 1.4 GHz radiometer frequencies with approximately 3-day revisit times. Both SMAP and SMOS provide near surface soil moisture (~0–5 cm) based on the L-band penetration depth. One major objective of the SMAP mission was to fuse the coarse resolution (~40 km) radiometric measurements with fine resolution (1–3 km) radar measurements (1.26 GHz) to produce soil moisture products at intermediate resolution (9 km) (Entekhabi et al., 2014). However, only the radiometric soil moisture products of SMAP are available following the failure of the SMAP radar on 7th July 2015. SMAP radar-based products are available for the first three months prior to the failure involving its high-power amplifier (HPA) (Neeck, 2015). Combining Sentinel-1 radar data with SMAP radiometric data is an approach employed as a solution to the SMAP radar failure (Das and Dunbar, 2018). The target accuracy of both SMAP and SMOS is $0.04 \text{ cm}^3/\text{cm}^3$. The accuracy of SMAP derived soil moisture has been demonstrated as $0.04 \text{ cm}^3/\text{cm}^3$ for both 36 km and 9 km gridded products (Chan et al., 2016, 2017; Colliander et al., 2017a). SMOS has demonstrated its expected accuracy of $0.04 \text{ m}^3/\text{m}^3$ at some of the sites (Al Bitar et al., 2012; Jackson et al., 2012). However, higher uncertainties in SMOS products have been observed in a number of other studies (Djamai et al., 2015; Pacheco et al., 2015; Niclòs et al., 2016). Despite their identical L-band frequencies and spatial and temporal resolutions, there are notable differences between SMAP and SMOS. SMOS measures surface emissions from a large number of view angles from 0 to 55° whereas SMAP measures surface emissions only at a 40° angle (Entekhabi et al., 2014; Karthikeyan et al., 2017b). Moreover, SMAP measures brightness temperatures with a better sensitivity with a noise-equivalent delta temperature (NEDT) $< 1 \text{ K}$ for 17-ms samples (Piepmeier et al., 2017) compared to SMOS, which has a sensitivity of $\sim 2\text{--}4.5 \text{ K}$ (Corbella et al., 2011). Furthermore, the SMAP and SMOS soil moisture products use different retrieval algorithms, model

Table 1
Summary of the datasets used in this study.

Dataset	Data type	Data source	Spatial resolution/ grid size	Temporal resolution	Accuracy	Period used in the study
SMAP 9 km enhanced radiometric soil moisture products (L3SMP-E)	Satellite	National Snow and Ice Data Center (NSIDC)	9 km	Daily global composites	0.04 v/v	2015/16
SMOS 25 km soil moisture products (CATDS L3 SM 3-DAY) (Product code: MIR_CLF33A and MIR_CLF33D)	Satellite	Centre Aval de Traitement des Données SMOS (CATDS)	25 km	Daily global composites	0.04 v/v	2015/16
MODIS Aqua LSTs (MYD11A1)	Satellite	Land Processes Distributed Active Archive Center (LP DAAC)	1 km	daily	± 1 K (Wan, 2008)	2005, 2015
MODIS Aqua 16-day NDVI composites (MYD13A2)	Satellite	Land Processes Distributed Active Archive Center (LP DAAC)	1 km	16-day	± 0.020	2003–2015
The National Airborne Field Experiment 2005 (NAFE05) soil moisture data	Airborne	http://www.nafe.newcastle.edu.au/sasmas/	1 km	Four consecutive Mondays	0.04–0.05 v/v (Gao et al., 2018)	31st Oct, 7th Nov, 14th Nov and 21st Nov 2005.
SASMAS in-situ data (0–5 cm soil profile)	In-situ	http://www.eng.newcastle.edu.au/sasmas/SASMAS/sasmas.htm	Point scale	20-min	± 0.01– ± 0.03 v/v for fine textured soils ± 0.3 °C	2003–2015
i. soil moisture ii. soil temperature	Modelled	Commonwealth Scientific and Industrial Research Organisation (CSIRO)	90 m	-	-	-
National Soil and Landscape Grid (Soil Grid)						
i. clay content						

Table 2

The land cover and soil texture of the SASMAS monitoring stations in Krui and Merriwa River catchments (modified from Kunkel et al., 2016).

Station	Land cover	Soil type	Clay%	Silt%	Sand%
K1	Crop/fallow	Loam	23	32	45
K2	Native pasture	Loamy sand	12	14	75
K3	Crop/fallow	Clay	71	16	13
K4	Native pasture	Clay	55	30	15
K5	Native pasture	Clay	64	20	16
K6	Improved Pasture	Clay loam	38	40	22
M1	Native pasture	Sandy loam	7	11	83
M2	Native pasture	Sand	0	0	100
M3	Native pasture	Clay loam	40	34	26
M4	Native pasture	Loam	29	41	30
M5	Native pasture	Clay	73	20	7
M6	Native pasture	Clay	72	20	8
M7	Improved Pasture	Clay loam	41	32	26
S1	Improved Pasture	Clay	55	35	10
S2	Native pasture	Clay loam	43	27	30
S3	Native pasture	Clay			
S4	Native pasture	Clay			
S5	Native pasture	Clay	47	34	19
S6	Native pasture	Clay	53	28	19
S7	Native pasture	Silt loam	19	41	40

parameters, some of the ancillary datasets (e.g. land cover maps) and assumptions (Al-Yaari et al., 2017; Karthikeyan et al., 2017b).

For downscaling, two different satellite products have been used in this study (Fig. 5). First, the SMAP Enhanced L3 Radiometer Global Daily 9 km EASE-Grid Soil Moisture, Version 2 (L3SMP-E) products over the Goulburn River catchment from April 2015 to September 2016 were obtained from the National Snow and Ice Data Center (NSIDC) (<http://nsidc.org/>). Here, Backus-Gilbert optimal interpolation techniques, the classical inversion method in microwave radiometry (Chaubell et al., 2016), have been used to retrieve maximum information from SMAP antenna temperatures and then converted into brightness temperatures (Chan et al., 2018; O'Neill et al., 2016). This interpolation process allows the preservation of the spatial resolution of the antenna gain function associated with the sampled radiometer data (Poe, 1990). The brightness temperatures have been resampled onto the 9-km Equal-Area Scalable Earth Grid, Version 2.0 (EASE-Grid 2.0) in a global cylindrical projection. Herein this dataset will be called as SMAP-E. The SMAP-E 9 km grid over the study area is shown in Fig. 5b. Secondly, the SMOS CATDS L3 SM 3-DAY, Release 4 soil moisture products (Product code: MIR_CLF33A and MIR_CLF33D) of 25 km grid size (CATDS, 2016; Al Bitar et al., 2017) were obtained from the Centre Aval de Traitement des Données SMOS (CATDS) (<https://www.catds.fr>). The CATDS Level 3 soil moisture products include daily ascending and descending multi-orbit retrievals, and their average was taken as the daily mean soil moisture in this study. The SMOS 3-day aggregation generates global L3 soil moisture on a 3-day sliding window at daily basis by performing a temporal aggregation of the L3 CATDS daily product. The soil moisture retrievals were resampled onto a 25-km Global Equal-Area Scalable Earth Grid (EASE grid) (Kerr et al., 2013). The SMOS 25 km grid is shown in Fig. 5c. It is noteworthy to mention that the spatial resolutions of the SMAP and SMOS soil moisture products stated in this article, i.e. SMAP-E 9 km and SMOS 25 km, are their grid posting resolutions, not the actual observation resolutions.

2.3. Other geospatial data

2.3.1. MODIS-derived NDVI and LST products

NDVI data over the Krui and Merriwa River catchments from 2003 to 2015 were obtained from MODIS/Aqua Vegetation Indices 16-Day L3 Global 1 km Grid V005 (MYD13A2) products (Didan, 2015) in order to classify the downscaling model based on different NDVI classes. MODIS/Aqua Land Surface Temperature and Emissivity (LST/E) Daily

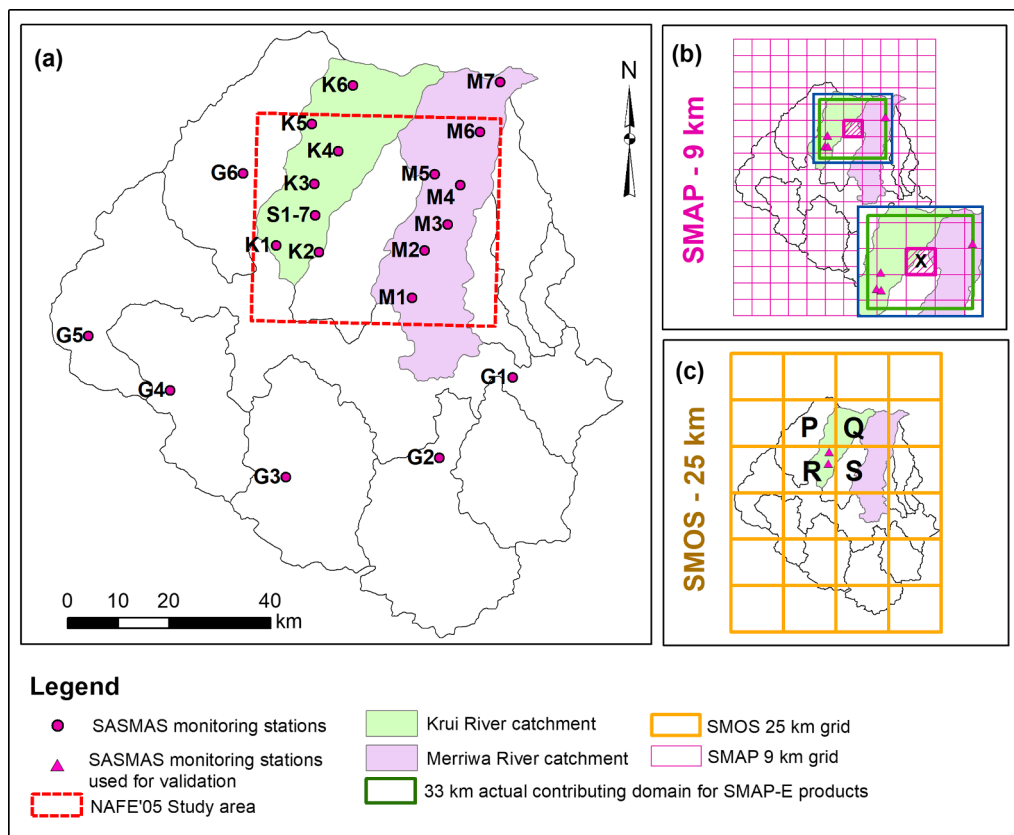


Fig. 5. The location of (a) NAFE'05 study area, (b) SMAP-Enhanced 9 km, and (c) SMOS 25 km grids over the Goulburn River catchment. The pixels used for validation are marked with letters (X for SMAP-E and P-S for SMOS).

L3 Global 1 km Grid V006 (MYD11A1) (Wan et al., 2015) dataset (1 km spatial resolution) was used in this study to derive daily night and day time LSTs over the Krui and Merriwa River catchments in 2015 and for the period of NAFE'05 (in 2005).

2.3.2. Soil and landscape grid national soil attributes maps

The clay content in the 0–50 mm soil profile over the Krui and Merriwa River catchments was extracted from the National Soil Attributes Maps of the Soil and Landscape Grid of Australia (Grundy et al., 2015). This is a new soils database for Australia released in late 2014, as a part of the GlobalSoilMap initiative. It provides quantitative soil properties on a 90 m grid for all of Australia. The Australian site data and spectroscopic estimates were used to develop the Soil and Landscape Grid dataset. The site data had been collected from 1931 to 2013 by the state and territory government agencies and Commonwealth Scientific and Industrial Research Organisation's (CSIRO) National Soil Archive and National Soil Database (NatSoil) to develop the National Soil Site Data Collection (NSSDC). The spectroscopic estimates were made with the National soil visible-near infrared database (NSVNIRD) to estimate soil properties, by using the soil samples collected for the National Geochemical Survey of Australia (Rossel et al., 2015). The clay content at 0–5 cm soil profile was used in this study for the regression tree as a modulating parameter of $\Delta T-\theta\mu$ relationship. Data from 15,192 NSSDC sites and 1113 NSVNIRD sites were used to develop the clay content maps in the Soil and Landscape Grid of Australia (Rossel et al., 2015). The uncertainties of the clay content of the top 5 cm soil layer is 18.5% with 14.1% and 23.0% at lower and upper 90% confidence limits, respectively (Rossel et al., 2015). The dataset was obtained from the Commonwealth Scientific and Industrial Research Organisation (CSIRO) data access portal (<https://data.csiro.au>).

2.3.3. NAFE'05 airborne dataset

Soil moisture retrievals from the NAFE'05 (Panciera et al., 2008) were used in this study to validate the downscaling algorithms. The NAFE'05 was conducted in November 2005 in the Goulburn River catchment to provide simulated SMOS observations from an L-band radiometer along with the soil moisture and other relevant ground observations. The objectives of the experiment were to develop the SMOS soil moisture retrieval algorithms, the SMOS downscaling approaches, and the assimilation of SMOS into land surface models for root zone soil moisture estimations. The regional airborne data collection was carried out in four consecutive Mondays starting from 31st October 2005 over a 40 km × 40 km area in the northern part of the catchment (Fig. 5a). The long drying period followed by the heavy rainfall on October 31st and November 1st allowed the NAFE'05 campaign to observe near surface soil moisture observations ranging from fully-saturated conditions to very dry conditions (Panciera et al., 2008). This covered the area cleared for cropping and grazing in the Krui and Merriwa River catchments where the SASMAS monitoring stations were concentrated, while the south-most part of the NAFE'05 study area included forested areas with dense vegetation. The Polarimetric L-band Multibeam Radiometer (PLMR) was employed for the regional NAFE'05 airborne data collection. The 1 km NAFE'05 soil moisture products were derived from PLMR brightness temperatures using a two channel inversion of the L-MEB model (Panciera et al., 2009). Although the nominal ground resolution of the dataset is 1 km, the pixel size varied from 860 to 1070 m due to the constant altitude of the flights above the median elevation over the varying terrain. The average flight altitude was 3000 m Above Ground Level (AGL) and the data was acquired in the morning between 6:00 h and 10:00 h along north–south orientated flight lines. Herein the term 'NAFE'05' is used in this paper to refer to this regional airborne campaign.

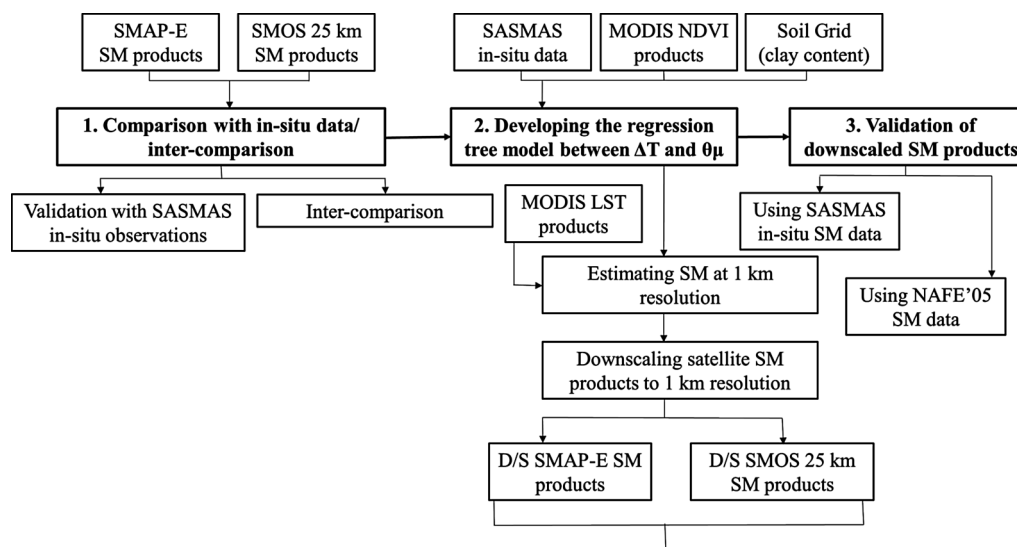


Fig. 6. Flow chart of the approach used to validate and downscale the satellite soil moisture products and to assess the reliability of the downscaled soil moisture products.

3. Methods

The methodology section consists of: (1) evaluation and inter-comparison of SMAP and SMOS products with in-situ data; (2) developing the regression tree model for downscaling; and (3) evaluation of the downscaled soil moisture data with SASMAS in-situ and NAFE'05 airborne observations. The overall approach is summarized in the flowchart shown in Fig. 6.

3.1. Evaluation and inter-comparison of SMAP-E and SMOS soil moisture products with in-situ data

The SASMAS in-situ soil moisture data from the top 5 cm soil profile was employed to evaluate near surface soil moisture measurements from SMAP-E and SMOS. Fig. 5 shows the distribution of SMAP-E 9 km and SMOS 25 km grids, as well as the SASMAS in-situ monitoring stations over the study area. Location details of the pixels used in this evaluation process are given in Table 3. The average of available in-situ observations of the top 5 cm over the SMAP and SMOS satellite footprints were used in this comparison. Note that the spatial averaging of limited in-situ observations can also contribute to the potential error in this comparison. This comparison was conducted over one SMAP-E 9 km pixel (X, Fig. 5b) and one SMOS 25 km pixel (R, Fig. 5c). Average soil moisture of three SASMAS monitoring stations over the nominal 33 km contribution domain (Fig. 5b) of the SMAP-E 9 km pixel X and two stations on SMOS 25 km pixel R (Fig. 5c) were employed in this comparison (Chan et al., 2018). Colliander et al. (2018) has employed a similar approach to validate SMAP-E products with core validation sites.

Then, the SMOS and SMAP-E soil moisture products over the Krui and Merriwa River catchments in 2015/16 were compared against each other over the four SMOS 25 km pixels, P, Q, R and S (Fig. 5c) by interpolating SMAP-E soil moisture to the SMOS 25 km grid centres. This

Table 3
Locations of the centroid of pixels used in the data validation process.

Dataset	Pixel	Longitude	Latitude
SMAP-E 9 km grid	X	150°15'52"E	31°59'50"S
SMOS 25 km grid	P	150°2'36"E	31°53'27"S
SMOS 25 km grid	Q	150°18'09"E	31°53'27"S
SMOS 25 km grid	R	150°02'36"E	32°07'17"S
SMOS 25 km grid	S	150°18'09"E	32°07'17"S

interpolation of SMAP-E into SMOS grid centres allows to capture a near approximation of average soil moisture from the actual contributing domain of SMAP-E.

3.2. Developing the downscaling model

The downscaling method presented in this paper is based on the soil thermal inertia relationship between ΔT and $\theta\mu$, which has been demonstrated by Fang et al. (2013, 2018) for multiple sites in United States. We first discuss the thermal inertia theory, and then present details on the regression tree model developed for this study.

Thermal inertia is a measure of the resistance of an objects temperature to the changes in its surrounding temperature (Sellers, 1965). The objects with high thermal inertia show a lower temperature change compared to the objects with low thermal inertia. Therefore, a low thermal inertia of soil shows a high variation in the diurnal temperature and vice versa. Accordingly, the relationship between the thermal inertia (TI) and ΔT can be given as (Engman, 1991):

$$\Delta T = f(1/TI), \quad (1)$$

$$\Delta T = T_{PM} - T_{AM}, \quad (2)$$

where T_{PM} and T_{AM} are the afternoon and early morning soil surface temperatures.

TI can also be defined as (Wang et al., 2010):

$$TI = \sqrt{\rho kc}, \quad (3)$$

where ρ is the bulk density (kg m^{-3}), k is the specific heat capacity ($\text{J kg}^{-1} \text{K}^{-1}$) and c is the thermal conductivity ($\text{W m}^{-1} \text{K}^{-1}$) of the material. Water has a high specific heat capacity compared to the dry soil. Therefore, the thermal inertia of wet soil is significantly higher than dry soil and exhibits lower diurnal temperature fluctuation. When the moisture content of the soil is increasing, the thermal inertia of the soil increases proportionally. Therefore, wet soils exhibit low diurnal soil temperature difference compared to dry soils (Verstraeten et al., 2006).

The relationship between the diurnal soil temperature difference and the daily mean soil moisture is complex and modulated by the season, vegetation density and the soil texture (Engman, 1991; Farrar et al., 1994; Peng et al., 2017; Sandholt et al., 2002). A regression tree model was used to represent this complex relationship. A basic regression tree algorithm typically produces a set of rules in a decision tree format, which can be used to represent the correlation between the

independent variable and the predictor variables under different conditions (De'ath and Fabricius, 2000). This approach does not require the assumption of a globally linear relationship, nor a priori knowledge of the mathematical form of nonlinear curve fitting methods (Breiman et al., 1984).

The downscaling method employed here is similar to the NLDAS product-based regression model developed by Fang et al. (2013, 2018) and Fang and Lakshmi (2014), but with in-situ data and additional factors. In this study, continuous long term in-situ observations of soil moisture and temperature were used together with a time series of remotely sensed NDVI data to develop the regression tree models by season. The in-situ data from the SASMAS network provided details on surface soil moisture change under different climatic conditions over the range of soil types. Soil texture information was also considered in the regression tree models, given the spatial variation in edaphic characteristics for this semi-arid study site and its implication for the spatio-temporal surface soil moisture dynamics (Chen et al., 2014; Cosh et al., 2008). In particular, a large portion of the study area is covered by vertisols, extensively swelling soils with high clay content. This type of soil shows large structural and volumetric changes during wetting, and this directly affects the soil water retention characteristics and near surface soil moisture (Rüdiger et al., 2005). The soils were classified into two classes as heavy clays (clay content > 35%) and other soils (Bonan, 2015). The soil clay content was considered as a modulating factor based on the effect of soil texture on the thermal conductivity, with thermal conductivity directly proportional to the thermal inertia (Engman, 1991).

The $\theta\mu$ and ΔT values of the top 5 cm soil profile at each monitoring station were calculated from the SASMAS in-situ dataset between 2003 and 2014. The ΔT values ($\Delta T = LST_{AM} - LST_{PM}$) were computed by using the LST difference between early morning and afternoon based on the approximate MODIS Aqua day and night overpass times over the study area, i.e. 01:30 (LST_{AM}) and 13:30 h (LST_{PM}). The NDVI (Tucker, 1979) was used in the regression tree model, to account for the impact of vegetation density in modulating soil temperature and soil moisture. The NDVI is defined as:

$$NDVI = (NIR - RED)/(NIR + RED) \quad (4)$$

where *NIR* and *RED* are the reflectance values from infrared and red bands respectively. NDVI values vary from -1 to $+1$, with negative values representing water, near zero values no vegetation cover (e.g., bare lands and urban areas), and values closer to $+1$ dense vegetation. Three NDVI classes were defined for the classification of the $\Delta T - \theta\mu$ regression model based on the vegetation density, i.e., $NDVI < 0.4$ (grasslands or no vegetation), $0.4 < NDVI < 0.6$ (abundant and vigorous vegetation), and $NDVI > 0.6$ (dense and vigorous vegetation) (de Alcântara Silva et al., 2016). The NDVI values at each station over the period of 2003–2014 were estimated by using MODIS 16-day NDVI composites (MYD13A2) (1 km resolution).

Lastly, the four Austral seasons, spring (from September to November), summer (from December to February), autumn (from March to May), and winter (from June to August), were used to classify the regression tree in view of the seasonal impact to the $\Delta T - \theta\mu$ relationship. In summary, the entire $\Delta T - \theta\mu$ regression model was classified into 24 classes, i.e. three NDVI classes, two soil classes and four seasonal classes. Fig. 7a shows the regression tree developed for the Austral spring. The regression tree for the other seasons were similarly developed.

The MODIS Aqua LST (MYD11A1) values over the Krui and Merriwa stations showed a strong linear relationship with the SASMAS observations in 2015 with a R^2 value of 0.74 at day time and 0.76 at night time. The day and night time MODIS Aqua LST (MYD11A1) values over SASMAS in-situ stations were compared against the top 5 cm SASMAS in-situ soil temperature values at approximate MODIS overpass times (13:30 h at day time and 01:30 h at night time). Consequently, MODIS day time and night time LST values were bias corrected using a linear

calibration with the SASMAS observations and subsequently used to calculate ΔT values at 1 km spatial resolution. The MODIS derived ΔT values were input into the regression tree to calculate respective $\theta\mu$ estimates at 1 km spatial resolution. The NDVI and soil clay content values at each 1 km ΔT pixel were extracted from the MODIS 16-day NDVI composites and the Soil and Landscape Grid National Soil Attributes Maps respectively.

The coarse resolution soil moisture products (θ_{SAT}) were thereafter downscaled to 1 km pixel p ($\theta_{ds, p}$) as:

$$\theta_{ds, p} = \theta_{est, p} + \left[\theta_{SAT} - \frac{1}{n} \sum_1^n \theta_{est, p} \right], \quad (5)$$

where $\theta_{est, p}$ is soil moisture content estimated by the regression tree at the 1 km pixel p , θ_{SAT} the satellite soil moisture product where p is laid within its foot print, and n is the total number of 1 km pixels ($p = 1..n$) within the coarse resolution satellite pixel.

3.3. Evaluation of the downscaled products

Evaluation of the downscaled soil moisture products and algorithms consisted of two parts: (1) assessing the accuracy of the downscaled products against the SASMAS in-situ observations during 2015; and (2) evaluating the consistency in spatial patterns between high resolution L-band airborne soil moisture retrievals and the downscaled soil moisture estimates derived from the upscaled airborne soil moisture retrievals.

3.3.1. Validating the downscaled products with SASMAS in-situ observations

The downscaled soil moisture products were compared with the SASMAS in-situ observations of the top 5 cm soil profile from K3, M6 and S3 stations in 2015. Due to the limited data availability, only a single station per downscaled pixel was compared; hence, subgrid-scale spatial variability of soil moisture within a downscaled pixel could not be assessed. However, in-situ soil moisture observations, albeit the limited availability, were assumed to be a reasonable representation of downscaled soil moisture products with the following reasons. First, SASMAS soil moisture monitoring sites are able to represent their surrounding landscape since they were established at carefully chosen 'time stable' locations (see Section 2.2.1). It is noteworthy to mention that the intensive field sampling conducted at the NAFE'05 and the careful positioning of stations supported the potential of using SASMAS data for upscaling to a large spatial extent to validate coarse resolution satellite soil moisture products without significant errors (Crow et al., 2012; Panciera et al., 2008; Rüdiger et al., 2003, 2007). Second, sub-grid spatial variability within the downscaled pixel deemed to be rather small. There existed very little difference in environmental factors (e.g., land cover, vegetation, soil type, topography, meteorological factors) that could contribute to large uncertainties in soil moisture within the spatial extent of downscaled pixel. Indeed, a multiscale analysis by Martinez et al. (2007) demonstrated very little soil moisture variability at a fine ($< 1 \text{ km}^2$) spatial scale based on intensive field campaigns conducted in this area during NAFE'05. Lastly, Chen et al. (2014) showed the temporal stability of the SASMAS network sites using the HYDRUS-1D soil water model. The sensitivity analyses revealed soil type and leaf area index as the key parameters affecting soil moisture variability through time. The calibrated model to a single site was able to simulate soil water storage for closely located monitoring sites as well as for distant sites (up to 30 km) if spatially variable rainfall was allowed. Chen et al. (2014) demonstrated the potential usefulness of continuous time, point-scale SASMAS in-situ observations and simulations for predicting the soil wetness status over a catchment of significant size (up to 1000 km^2) across scales. Note that relative metrics (see Section 3.3.3) were used in this validation process, due to the low density of in-situ soil moisture monitoring stations.

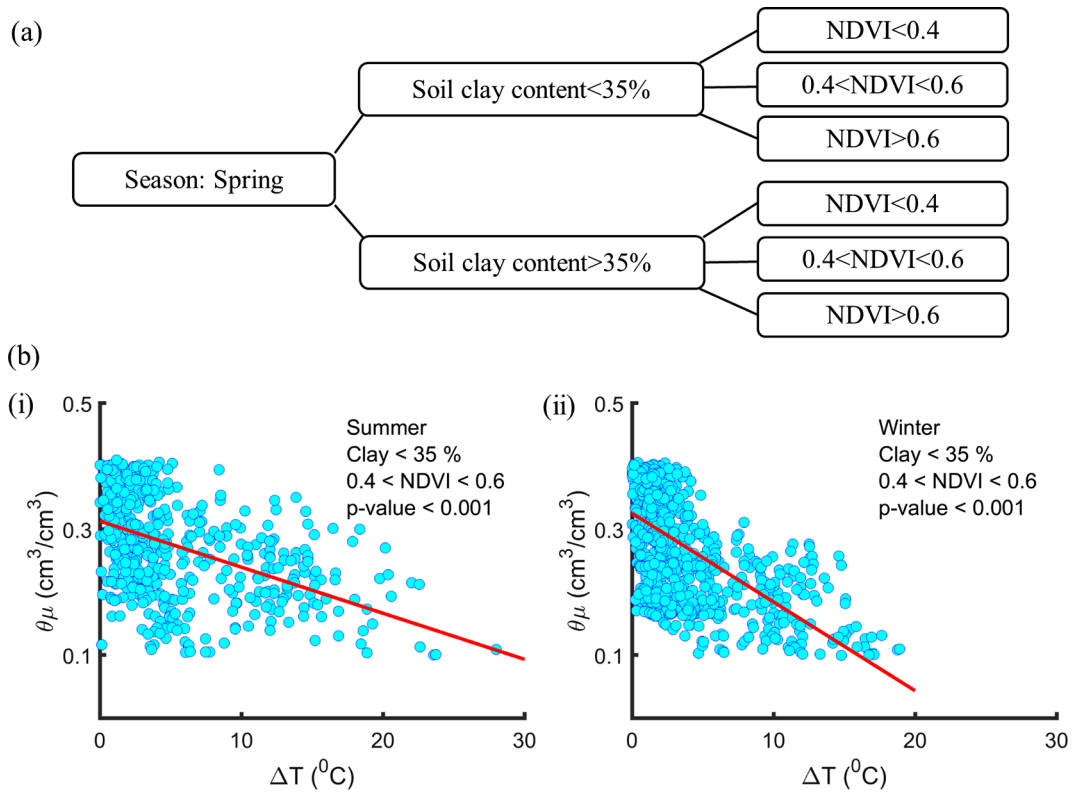


Fig. 7. (a) The regression tree developed for the Austral spring. The ΔT and θ_{μ} values were classified based on the season, soil clay content and the NDVI value as shown in the regression tree. (b) Regression Models developed for the class of clay < 35% and 0.4 < NDVI < 0.6 for (i) Austral summer, and (ii) Austral winter seasons.

3.3.2. Validating the downscaling algorithms using NAFE'05 airborne observations

One major problem in validating downscaled soil moisture products with sparse in-situ networks is the large spacing between the monitoring stations. When in-situ observations are used as reference observation to assess downscaled products, several problems could arise from resolution cell representation, station-to-station biases, and consistency of data records (Colliander et al., 2017b). Use of high spatial resolution airborne soil moisture observations as reference observations has been considered as a robust, alternative approach to validate spatial downscaling methods (Colliander et al., 2017b; Merlin et al., 2008; Piles et al., 2009; Wu et al., 2017). Due to unavailable resources, the field experiment to collect a set of high resolution airborne soil moisture observations could not be conducted during the study period. Instead, our downscaling algorithms were further tested with the NAFE'05 airborne soil moisture dataset over the 40 km × 40 km study area covering Krui and Merriwa River catchments as follows. This is the only high resolution airborne soil moisture dataset available in our study area. The ~1 km resolution airborne soil moisture data were first upscaled by taking the spatial mean over the study area to simulate a coarse resolution satellite soil moisture pixel. The aggregated soil moisture data were then downscaled to 1 km using the developed regression tree models (Eq. (5)) with MODIS-derived NDVI and LST datasets. If the LST datasets had significant spatial data gaps due to the clouds on the NAFE'05 campaign days, the LST data prior to or just after the campaign days were used assuming no significant variation in the daily soil moisture between adjacent dates. Then, the spatial patterns of the downscaled soil moisture were compared against the NAFE'05 1 km resolution airborne soil moisture data and the absolute difference between the two datasets was calculated for each day. The region covered by the dense vegetation along the southern border of the NAFE'05 study area was masked and excluded from this analysis (Fig. 8a). The data from 31st October 2005 was not considered in this comparison due to

the large data gaps caused by the cloud cover.

3.3.3. Performance metrics

The RMSE, ubRMSE, coefficient of determination (R^2), Pearson's correlation coefficient (R) and coefficient of variation (CV) were used as metrics in data comparisons. These metrics are computed as (Entekhabi et al., 2010b; Colliander et al., 2018):

$$RMSE = \sqrt{\frac{\sum_{i=1}^n (\theta_{ds,i} - \theta_{obs,i})^2}{n}}, \quad (6)$$

$$ubRMSE = \sqrt{\frac{\sum_{i=1}^n ((\theta_{ds,i} - \bar{\theta}_{ds}) - (\theta_{obs,i} - \bar{\theta}_{obs}))^2}{n - 1}}, \quad (7)$$

where $\theta_{obs,i}$ is the i^{th} value of soil moisture observations (in-situ or airborne) used in these comparisons as the true values, $\theta_{ds,i}$ the i^{th} value of the downscaled 1 km soil moisture products and n is the number of observations. $\bar{\theta}_{obs}$ and $\bar{\theta}_{ds}$ are the means of observed and downscaled soil moisture, respectively.

The R^2 value, R and CV are estimated as:

$$R^2 = 1 - \frac{\sum (\theta_i - \theta_{reg,i})^2}{\sum (\theta_i - \bar{\theta})^2}, \quad (8)$$

$$R = \frac{1}{(n - 1)} \sum_{i=1}^n \left(\frac{\theta_{ds,i} - \bar{\theta}_{ds}}{s_{ds}} \right) \left(\frac{\theta_{obs,i} - \bar{\theta}_{obs}}{s_{obs}} \right), \quad (9)$$

$$CV = \frac{s}{\bar{\theta}}, \quad (10)$$

where $\theta_{reg,i}$ is the predicted soil moisture from a regression fit between θ_{ds} and θ_{obs} , s_{ds} and s_{obs} are the standard deviations of downscaled and observed soil moisture values, respectively. The standard deviation (s) is estimated by:

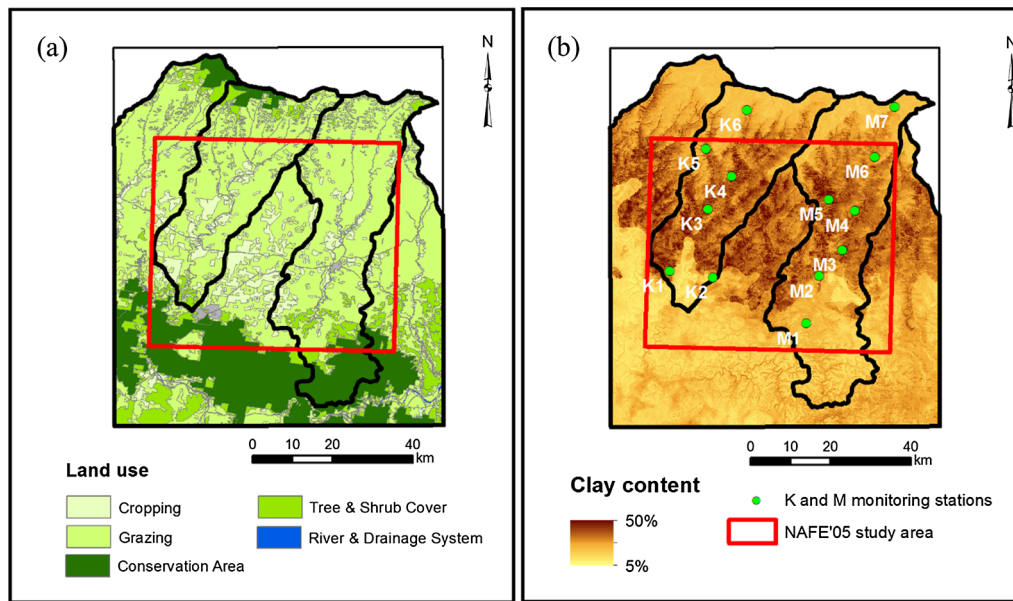


Fig. 8. (a) Land use/land cover, and (b) soil clay content over the NAFE'05 study area. The dense vegetation belt across the southmost region of the NAFE'05 study area can also be identified as a divide of soil texture.

$$s = \sqrt{\frac{\sum_{i=1}^n (\theta_i - \bar{\theta})^2}{n-1}} \quad (11)$$

Here, θ_i is the soil moisture estimate at the i^{th} observation ($i = 1:n$) and $\bar{\theta}$ is the spatial or temporal mean of the soil moisture estimates.

4. Results

4.1. Comparison of coarse resolution satellite soil moisture products

The comparisons between the in-situ observations and satellite soil moisture products are shown in Fig. 9. Fig. 9a shows the agreement between SMAP-E products and the SASMAS in-situ data at SMAP-E pixel X (Fig. 5b), along with the daily precipitation measured at the K3 station. The response of SMAP soil moisture to the precipitation is evident in Fig. 9. The SMAP-E soil moisture product showed a good agreement with the in-situ data at pixel X showing an ubRMSE value of 0.051 and R^2 values of 0.73 (Fig. 9a). However, a slight underestimation was observed from the SMAP products when compared with the in-situ data, particularly during the drying stage. Chen et al. (2017) also explain an underestimation bias in SMAP data, especially in drying conditions, possibly caused by the mismatch between the measuring depths of in-situ sensors and L-band penetration depths. The SMOS soil moisture products showed a notable underestimation when compared against SASMAS in-situ observations (Fig. 9b) at pixel R (Fig. 5c). The temporal pattern of soil moisture (i.e. climatology) was reasonably captured by the SMOS products (Fig. 9b). An ubRMSE of $0.056 \text{ cm}^3/\text{cm}^3$ with R^2 value of 0.64 was found between SMOS 25 km gridded product and in-situ data at this pixel. The limited in-situ observations along with the errors in spatial averaging and instrument errors in in-situ data were also potential error sources in these comparisons between satellite soil moisture products and in-situ observations. The underestimation is less evident in SMAP compared to SMOS soil moisture products. A number of studies have observed the same behaviour of a general under-estimation with SMOS (Al Bitar et al., 2012; Dall'Amico et al., 2012; Gherboudj et al., 2012; Cui et al., 2017; Dente et al., 2012; Pacheco et al., 2015; Niclòs et al., 2016). Some of the possible reasons for the SMOS underestimation can be identified as; the L-band penetration depth being less than 5 cm for wet soils (Ulaby et al., 1986), inability to represent spatial heterogeneity at the coarser resolution, in-situ measurements overestimating the soil moisture,

systematic bias created by the retrieval algorithm and the erroneous ancillary data such as soil texture and land use (Al Bitar et al., 2012). The improved instrument design and algorithm of SMAP (Karthikeyan et al., 2017b) can also contribute to the better accuracy of SMAP.

The comparison between SMOS and SMAP-E soil moisture products over the SMOS pixels P, Q, R and S shows a reasonably good agreement with RMSEs of 0.089, 0.075, 0.072 and $0.072 \text{ cm}^3/\text{cm}^3$ ($R^2 = 0.58, 0.57, 0.69$ and 0.68 , p-values < 0.001 for all cases) over the SMOS 25 km pixels P, Q, R and S, respectively (Fig. 10).

4.2. Development of the downscaling model

The regression fits developed for the class with clay $< 35\%$ and $0.4 < \text{NDVI} < 0.6$ for Austral summer and winter are shown in Fig. 7 (i) and (ii). Around 20,000 ($\Delta T, \theta\mu$) data pairs obtained from ten SASMAS stations from 2003 to 2014 were used to develop the regression tree model, based on the availability of reliable near surface (0–5 cm) datasets. The large sample size collected over different climate conditions was sufficient to capture the variability as required by the regression tree classification.

4.3. Validating the downscaled products with in-situ data

Fig. 11a shows the comparison of the downscaled soil moisture products of SMAP-E km, and SMOS, with the in-situ observations at K3, M6, and S3 stations. The top 5 cm soil moisture data were unavailable at the other SASMAS stations in 2015. Therefore, the only option was to compare the downscaled data with the available in-situ measurements, although these three monitoring stations are laid within separate 1 km pixels. The downscaled soil moisture estimates of the satellite products, SMAP-E and SMOS, have captured the temporal variability of soil moisture with a good accuracy at all stations (Fig. 11a). At the M6 monitoring station, the downscaled products showed a general underestimation compared to the in-situ record. Lack of spatial representativeness of M6 station and instrument errors can be possible causes for this mismatch. Fig. 11b shows the agreement between the in-situ data and downscaled soil moisture estimates of SMAP-E and SMOS products. These downscaled SMAP-E and SMOS soil moisture products showed average ubRMSE values of 0.068 and $0.051 \text{ cm}^3/\text{cm}^3$ (with average R^2 values of 0.40 and 0.61), respectively.

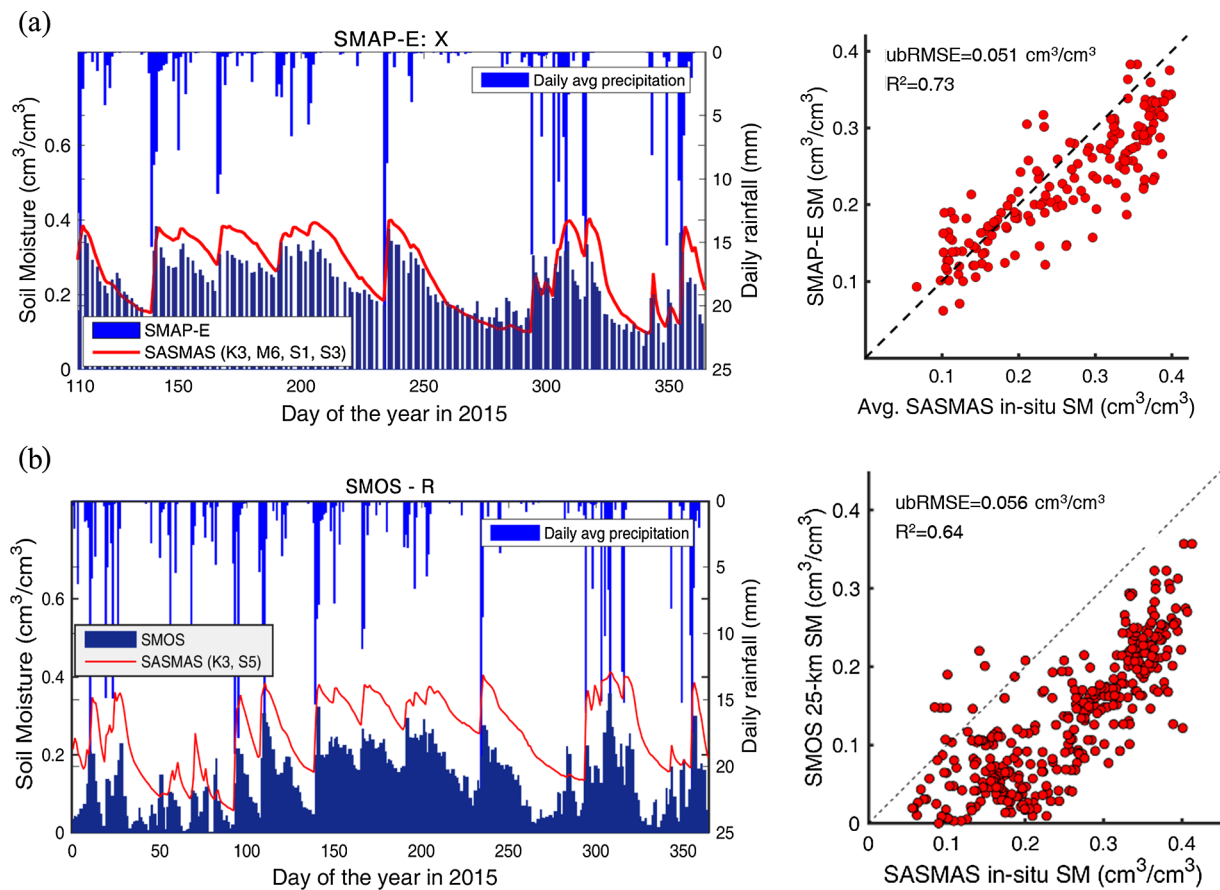


Fig. 9. Comparison of the temporal patterns and agreement between SASMAS in-situ observations at top 5 cm soil profile and (a) SMAP-E, and (b) SMOS soil moisture products. The daily precipitation shown in the figure is based on the in-situ observations at SASMAS K3 monitoring station.

Table 4 shows a summary of the agreement between the SASMAS in-situ observations and the downscaled soil moisture product at stations K3, M6, and S3. Downscaled SMOS products show better ubRMSE values and high R^2 against in-situ data, compared to the downscaled SMAP-E products. Fig. 12 illustrates the spatial variability of soil moisture over the Krui and Merriwa River catchments, as captured by the SMAP-E and SMOS soil moisture products and their downscaled

counterparts on 28th June 2015. This epoch was selected due to little cloud cover of the MODIS LST scene. When compared to the coarse resolution soil moisture products, it is evident that the downscale products have captured the sub-catchment level spatial variability of soil moisture at a much finer scale. It can be seen that the wet pixels in the middle of the Krui River catchment and the northern half of the Merriwa River catchment (Fig. 12) are closely related to the clay

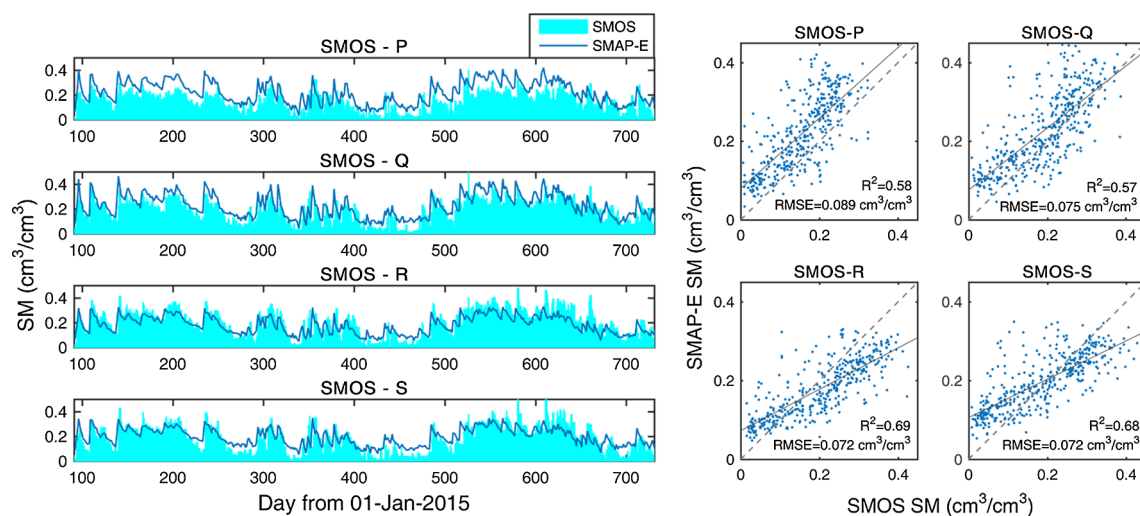


Fig. 10. Comparison and correlation between SMOS and SMAP-E soil moisture products over Krui and Merriwa River catchments in 2015/16.

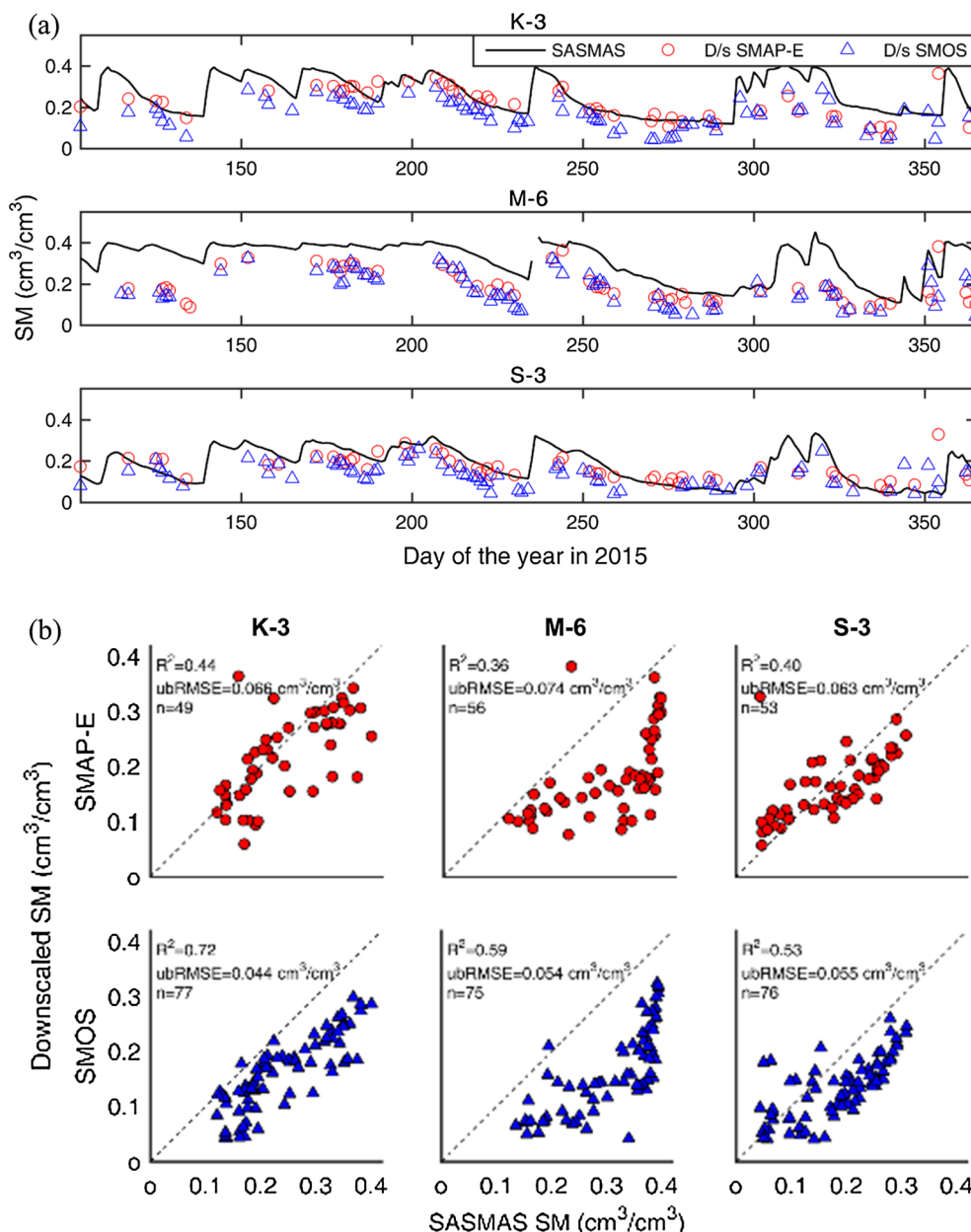


Fig. 11. (a) Temporal variability of soil moisture as captured by the downscaled SMAP-E 9 km, and SMOS 25 km gridded products with respect to SASMAS in-situ data at stations K-3, M-6, and S-3. (b) The agreement between the downscaled SMAP-E, and SMOS soil moisture products with SASMAS in-situ data.

Table 4
Agreement between SASMAS in-situ data and downscaled satellite soil moisture data at monitoring stations K3, M6 and S3.

Downscaled product	SASMAS monitoring station					
	K-3		M-6		S-3	
	ubRMSE (cm ³ /cm ³)	R ²	ubRMSE (cm ³ /cm ³)	R ²	ubRMSE (cm ³ /cm ³)	R ²
D/s SMAP-E	0.066	0.44	0.074	0.36	0.063	0.40
D/s SMOS	0.044	0.72	0.054	0.59	0.055	0.53

content of the soils (Fig. 2a). The increasing soil moisture gradient towards north, driven by the precipitation patterns and soil texture, is visible in the downscaled products. The subpixel scale spatial patterns of SMOS and SMAP soil moisture are similar, since these patterns are

based on the soil moisture estimates derived from MODIS LSTs.

4.4. Validating the downscaling algorithms with the NAFE'05 airborne observations

Fig. 13a shows the distribution of the NAFE'05 soil moisture data of the regional airborne campaign on 7th November, 14th November and 21st November 2005, with corresponding downscaled soil moisture estimates. Soil moisture variability of 31st October 2005 was excluded in this figure due large data gaps caused by clouds. The NAFE'05 regional soil moisture datasets of the four subsequent campaign days showed spatial means of 0.44, 0.36, 0.16 and 0.14 cm³/cm³ with CVs of 0.32, 0.37, 0.63 and 0.60 respectively over the 40 × 40 km study area. This clearly showed a drying trend from 7th November to 21st November 2005. The SMAP-E soil moisture products show a mean value of 0.20 cm³/cm³ (standard deviation of 0.07 cm³/cm³) over the NAFE'05 study area during 2015 and 2016. The spatial average of the NAFE soil

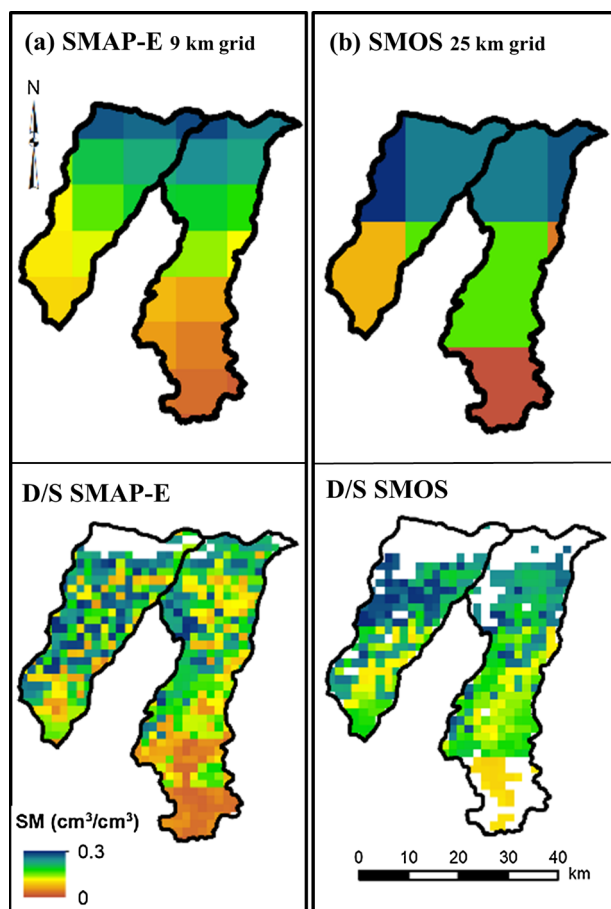


Fig. 12. The spatial variability of soil moisture as captured by the coarse resolution satellite soil moisture products and their downsampled counterparts of (a) SMAP-E 9 km, and (c) SMOS 25 km gridded products on 28th June 2015 over the Krui and Merriwa River catchments.

moisture data in the $40 \text{ km} \times 40 \text{ km}$ study area over the 4 days showed a mean value of $0.27 \text{ cm}^3/\text{cm}^3$ (standard deviation = $0.15 \text{ cm}^3/\text{cm}^3$). This shows that the NAFE'05 data shows slightly high soil moisture content compared to the soil moisture content as measured by the SMAP over the two years, yet displaying the typical soil moisture conditions of the area.

The downsampled data showed mean soil moisture values close to the NAFE'05 observations, but with less variability (Fig. 14). The response from the saturated clay soils and the surface runoff, caused by the early morning precipitation events is a probable reason for the high variability in NAFE'05 datasets. The SASMAS in-situ data shows precipitation of $\sim 20 \text{ mm}$ at S2 on 30th and 31st October 2005. This included light precipitation events ($\sim 12 \text{ mm}$) in the early morning of 31st October, i.e., a couple of hours before the flight time. This resulted in wet conditions on 31st October 2005 observed from the NAFE'05 dataset. In addition, the precipitation events on 31st October 2005 (Table 5) caused large data gaps in the MODIS LST due to the dense cloud cover on this day. A 12 mm precipitation event was also recorded at S2 on 5th November 2005 which explains the higher mean soil moisture values observed from the NAFE'05 dataset compared to the average of the SMAP soil moisture products over this area during 2015/16. Furthermore, Table 5 shows a general gradient of precipitation towards north across the NAFE'05 study area. This can be a possible reason for the higher soil moisture values in the northern part of the NAFE'05 area compared to the southern part. The response from surface runoff and soil saturation can also be identified as possible reasons for the extreme wet pixels in the NAFE'05 dataset.

Fig. 13 shows a good agreement in the spatial patterns between

NAFE'05 data and downsampled soil moisture products. The lower soil moisture values resulting from the high sand content in the southern part of the $40 \text{ km} \times 40 \text{ km}$ NAFE'05 area (i.e. the southern parts of the Krui and Merriwa River catchments) and the high soil moisture values resulting from the high clay content in the mid-regions of the two sub-catchments (Fig. 8b) were evident in both downsampled and NAFE'05 maps, especially during the dry conditions on 21st November 2005 (Fig. 13a). This highlights soil texture as a dominant factor regulating spatial patterns of soil moisture in the study area. This is compatible with the findings of Martinez et al. (2007) at the Stanley catchment, explaining that the wettest areas of the catchment are dominated by the clay soils.

The error maps shown in Fig. 13b illustrate the absolute error between observed and downsampled datasets of the NAFE'05. The two datasets have a reasonable agreement showing an error $< 0.1 \text{ cm}^3/\text{cm}^3$ for more than 80% of the area on 7th and 14th November 2005. Over 95% of the area shows an error less than $0.1 \text{ cm}^3/\text{cm}^3$ on 21st November 2005 under the dry conditions. Higher error values ($> 0.1 \text{ cm}^3/\text{cm}^3$) can be seen in the wetter pixels, possibly caused by higher precipitation in the northern part of the study area. A better agreement can be seen between the two datasets with increasing catchment dryness (Figs. 13 and 14). Overall, the comparison between NAFE'05 and downsampled soil moisture datasets show an average RMSE of $0.07 \text{ cm}^3/\text{cm}^3$ (with R value of 0.4).

5. Discussion and conclusion

This paper explored the feasibility of generating a time record of soil moisture at high spatial resolution (1 km) using SMAP-E 9 km and SMOS 25 km gridded satellite soil moisture products over two semi-arid river catchments in the Upper Hunter Region of New South Wales, Australia. The soil moisture and soil temperature dataset for the top 5 cm soil layer, obtained from the in-situ soil moisture network (SASMAS) over the Goulburn River catchment, was used to develop a thermal inertia based regression tree model between ΔT and $\theta\mu$. The regression tree model was classified based on the modulating factors; season, vegetation density and soil texture. The MODIS LST products were then used to estimate soil moisture at 1 km resolution from the coarse satellite products using the rule-based regression tree model. The accuracy of the downsampled soil moisture products was evaluated by using the SASMAS in-situ and the NAFE'05 airborne datasets.

Both SMAP-E and SMOS soil moisture products showed a temporal change consistent with the precipitation. SMAP-E soil moisture showed an agreement with the in-situ data of $0.051 \text{ cm}^3/\text{cm}^3$ ubRMSE ($R^2 = 0.73$), which is slightly higher than the accepted SMAP accuracy of $0.04 \text{ cm}^3/\text{cm}^3$. The SMOS 25 km gridded product showed ubRMSE of $0.056 \text{ cm}^3/\text{cm}^3$ ($R^2 = 0.64$) against in-situ data. The unavailability of evenly and densely distributed in-situ stations over the SMAP-E footprint are a major limitation of this comparison. Besides the measurement errors from the in-situ sensors ($\sim 0.03 \text{ cm}^3/\text{cm}^3$), soil cracking over the clay soils was a serious issue for the near surface ($0\text{--}5 \text{ cm}$) soil moisture monitoring. In the dry periods, the cracks caused sensors to be not in contact with the soils, whereas after precipitation, the soils get flooded and swelled. This creates a challenge for maintaining near surface sensors and assuring the data quality for in-situ observations. The limited availability of in-situ observations and the error in spatial averaging of in-situ data over the satellite footprints are the main sources of errors in this comparison. Because of the limited availability of the top 5 cm soil moisture observations, Senanayake et al. (2017) tested the proposed downscaling approach with the in-situ data of $0\text{--}30 \text{ cm}$ soil layer. Soil moisture and temperature data from five Krui River catchment monitoring stations in 2015 (~ 1700 data pairs) were employed in this work, based on the premise that the daily mean of the near surface soil moisture ($0\text{--}5 \text{ cm}$) was closely related to the daily mean soil moisture of the $0\text{--}30 \text{ cm}$ soil layer in the study area (Martinez et al., 2007). This study showed an RMSE of $0.14 \text{ cm}^3/\text{cm}^3$ when the

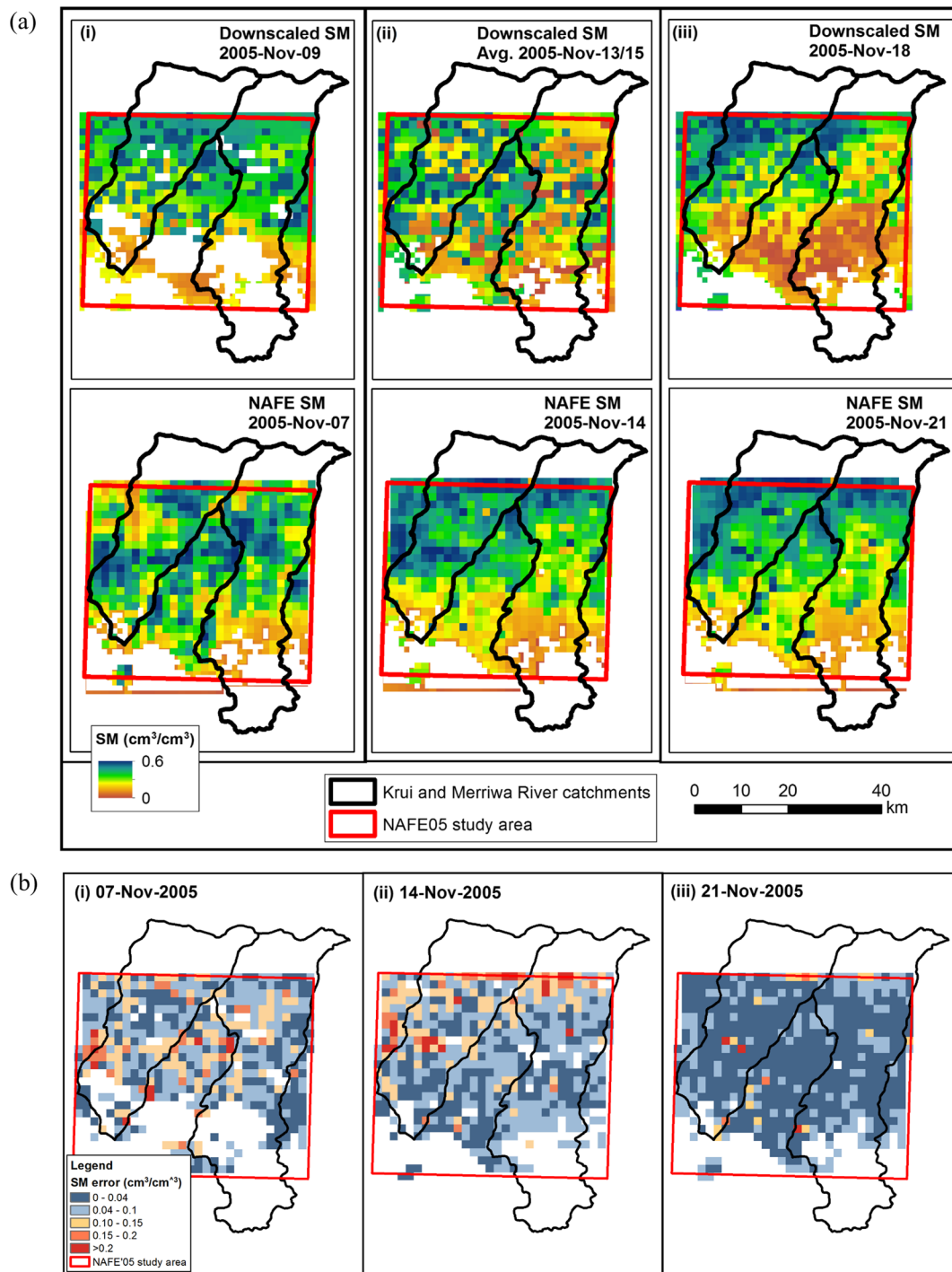


Fig. 13. (a) Comparison of the downscaled soil moisture products with NAFE'05 regional airborne data collection. The downscaled products of the closest date to the NAFE'05 regional airborne data collection were used in this comparison based on the cloud effect on MODIS LSTs. (b) The absolute difference between the soil moisture of NAFE'05 airborne dataset and downscaled products on 7th November, 14th November and 21st November 2005 over the NAFE'05 study area. Data from 31st October 2005 was excluded in this figure due to high cloud cover.

downscaled data were compared against the in-situ observations.

The downscaled soil moisture products of the SMAP-E and SMOS showed uRMSEs of 0.068 and 0.051 cm^3/cm^3 , respectively, with the SASMAS in-situ observations. The accuracy of the coarse resolution satellite soil moisture products directly affects the accuracy of their downscaled counterparts. It is noteworthy to mention that, the average of the downscaled soil moisture products within a coarse resolution satellite footprint was the same as the original value of the coarse resolution satellite soil moisture product (see Eq. (5)). The errors in

MODIS LSTs (Wan, 2008) and the uncertainties in clay content values (Rossel et al., 2015) can also be identified as possible sources of errors.

Lack of in-situ network sites within 1 km pixel was a major limitation in validating the downscaled soil moisture products. Therefore, presenting metrics for absolute soil moisture (i.e. RMSE and bias) is invalid. Accordingly, relative metrics were used in presenting the results of this validation (i.e. uRMSE and correlation). In addition, NAFE'05 data was also used in this study as a solution to lack of ground measurements for validation. The downscaled soil moisture showed a

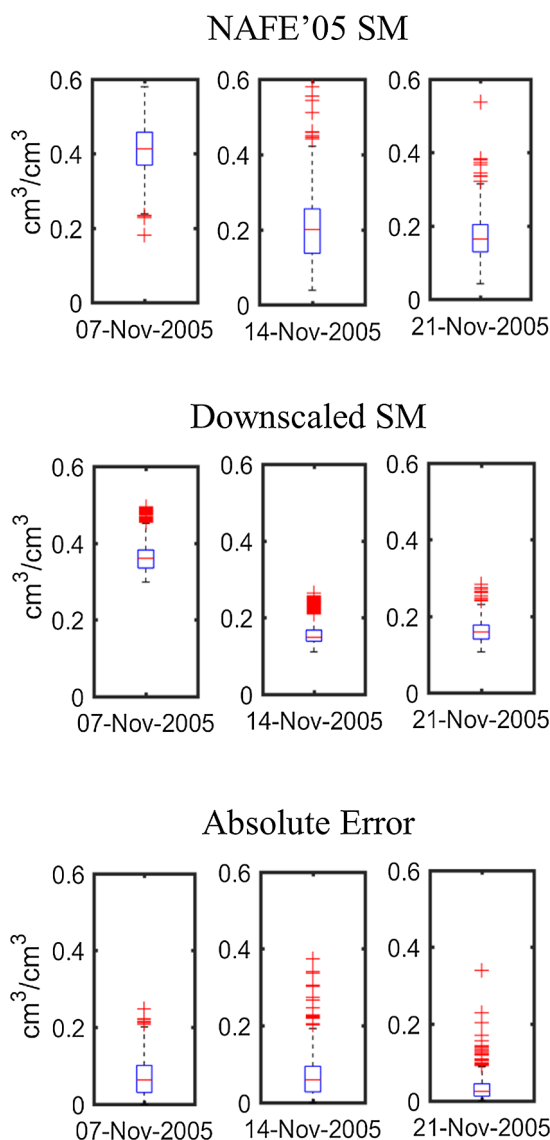


Fig. 14. The distribution of NAFE'05 and downscaled soil moisture with the absolute error between the two datasets over the 40 km × 40 km study area on 7th November, 14th November and 21st November 2005.

Table 5
Weekly precipitation data recorded at the SASMAS monitoring stations during the period of NAFE'05 regional airborne campaign.

Week	Precipitation (mm)					
	Krui River catchment			Merriwa River catchment		
	S2	K4	M1	M3	M4	M5
25 Oct – 31 Oct	17.0	18.2	22.0	11.8	19.0	16.6
1 Nov – 7 Nov	14.4	18.2	12.4	23.2	23.2	35.4
8 Nov – 14 Nov	11.0	8.4	1.4	5.0	11.2	8.8
15 Nov – 21 Nov	0	0	0.2	0	0	0

good agreement with the spatial patterns shown by NAFE'05 airborne campaign. Both NAFE'05 and downscaled data shows the spatial patterns driven by soil texture. The clay-rich mid-catchment areas of the Krui and Merriwa River (Fig. 8b) can be distinguished from the north and south-most regions in the soil moisture maps (Fig.13a). This agrees

with the findings of the previous studies (Cosh et al., 2008; Cantón et al., 2004; Gómez-Plaza et al., 2000) that have shown soil properties and vegetation as the main factors affecting soil moisture variability in semi-arid regions. The results show that the algorithms work well over both spatially and temporally dry conditions compared to wet conditions. Another major limitation of this downscaling method is the data gaps in MODIS LST occurred due to the cloud cover. One possible approach to address this problem is by using the LST products from geostationary satellites (Oyoshi et al., 2014; Yamamoto and Ishikawa, 2018). Although their spatial resolution is slightly coarser than MODIS LST products, the high temporal resolution of the geostationary LST data allows the retrieval of close representations of T_{AM} and T_{PM} . The 4 km spatial and one-hour temporal resolution of Multi-functional Transport Satellite (MTSAT)-1R (Himawari-6) LSTs can be shown as an example dataset of LST. However, use of geostationary satellites do not completely ensure to avoid data gaps along a day due to the presence of clouds. Piles et al. (2016) have proposed a technique to improve the spatio-temporal resolution of soil moisture from the synergy of SMOS and Meteosat Second Generation (MSG) Spinning Enhanced Visible and Infrared Imager (SEVIRI) observations. SEVIRI is a geostationary orbit optical imaging radiometer on-board the MSG satellite. Soil moisture retrievals from SMOS with LST and Fractional Vegetation Cover (FVC) products from the SEVIRI have been employed in this approach. In addition, Djamaï et al. (2016) proposed a method to estimate soil moisture at high resolution on cloudy days, by combining the Canadian Land Surface Scheme (CLASS) with DisPATCH model. This involves interpolating the input data of CLASS at high resolution by kriging and subsequent near surface soil moisture simulation and calibrating the CLASS using the downscaled soil moisture from DisPATCH model. Another potential way of filling these data gaps caused by the cloud cover is using the persistent spatial patterns of soil moisture. A number of researchers have studied the temporal persistence of soil moisture patterns (Vanderlinden et al., 2012; Brocca et al., 2009; Gómez-Plaza et al., 2000; Cosh et al., 2008). However, the spatial pattern of catchment soil moisture can be changed based on the factors such as precipitation pattern, seasonal vegetation dynamics and mean catchment wetness (Famiglietti et al., 2008; Chen et al., 2014). Therefore, comprehensive studies on time stability of soil moisture is required prior to such approach.

The methodology introduced in this study shows a good potential in producing a time series record of high-resolution soil moisture over arid and semi-arid regions. Future studies should be directed on further refining the regression algorithms by combining model-derived datasets and other forcing factors.

6. Declarations of interest

None.

Acknowledgements

This research was funded by the University of Newcastle Postgraduate Research Scholarship (UNRSC) 50:50, the Australian Research Council (ARC)'s Discovery Projects funding scheme (# DP170102373) and the United States NASA GRACE Science Project (# NNX14AD70G). We appreciate constructive comments and suggestions from Dr. Rajat Bindlish, Research Physical Scientist at the NASA Goddard Space Flight Center, Greenbelt, MD, United States and from Dr. Yann H. Kerr, Director of Centre d'Etudes Spatiales de la Biosphère (CESBIO) and Principal Investigator of the SMOS project. The insightful comments and feedback from the three anonymous reviewers greatly improved the quality of this paper.

References

- Al Bitar, A., Leroux, D., Kerr, Y.H., Merlin, O., Richaume, P., Sahoo, A., Wood, E.F., 2012. Evaluation of SMOS soil moisture products over continental US using the SCAN/SNOTEL network. *IEEE Trans. Geosci. Remote Sens.* 50 (5), 1572–1586.
- Al Bitar, A., Mialon, A., Kerr, Y.H., Cabot, F., Richaume, P., Jacquette, E., Quesney, A., Mahmoodi, A., Tarot, S., Parrens, M., Al-Yaari, A., Pellarin, T., Rodriguez-Fernandez, N., Wigneron, J.P., 2017. The global SMOS Level 3 daily soil moisture and brightness temperature maps. *Earth Syst. Sci. Data* 9 (1), 293–315.
- Al-Yaari, A., Wigneron, J.-P., Kerr, Y., Rodriguez-Fernandez, N., O'Neill, P., Jackson, T.J., De Lannoy, G.J.M., Al Bitar, A., Mialon, A., Richaume, P., Walker, J.P., Mahmoodi, A., Yueh, S., 2017. Evaluating soil moisture retrievals from ESA's SMOS and NASA's SMAP brightness temperature datasets. *Remote Sens. Environ.* 193, 257–273.
- Barré, H.M., Duesmann, B., Kerr, Y.H., 2008. SMOS: the mission and the system. *IEEE Trans. Geosci. Remote Sens.* 46 (3), 587–593.
- Boening, C., Willis, J.K., Landerer, F.W., Nerem, R.S., Fasullo, J., 2012. The 2011 La Niña: so strong, the oceans fell. *Geophys. Res. Lett.* 39 (19).
- Bonan, G., 2015. *Ecological Climatology: Concepts and Applications*. Cambridge University Press.
- Breiman, L., Friedman, J.H., Olshen, R.A., Stone, C.J., 1984. *Classification and Regression Trees (The Wadsworth Statistics and Probability Series)*. Wadsworth Publishing Co Inc, Belmont, California.
- Brocca, L., Melone, F., Moramarco, T., Morbidelli, R., 2009. Soil moisture temporal stability over experimental areas in Central Italy. *Geoderma* 148 (3), 364–374.
- Brocca, L., Ciabatta, L., Massari, C., Camici, S., Tarpanelli, A., 2017. Soil moisture for hydrological applications: open questions and new opportunities. *Water* 9 (2), 140.
- Cantón, Y., Solé-Benet, A., Domingo, F., 2004. Temporal and spatial patterns of soil moisture in semiarid badlands of SE Spain. *J. Hydrol.* 285 (1–4), 199–214.
- Carlson, T., 2007. An overview of the “triangle method” for estimating surface evapotranspiration and soil moisture from satellite imagery. *Sensors* 7 (8), 1612–1629.
- Carlson, T.N., Gillies, R.R., Perry, E.M., 1994. A method to make use of thermal infrared temperature and NDVI measurements to infer surface soil water content and fractional vegetation cover. *Remote Sens. Rev.* 9 (1–2), 161–173.
- CATDS, 2016. CATDS-PDC L3SM Aggregated - 3-day, 10-day and monthly global map of soil moisture values from SMOS satellite. CATDS (CNES, IFREMER, CESBIO). < <https://doi.org/10.12770/b57e0d3d-e6e4-4615-b2ba-6feb7166e0e6> > . [Accessed March 27, 2017].
- Chan, S.K., Bindlish, R., O'Neill, P.E., Njoku, E., Jackson, T., Colliander, A., Chen, F., Burgin, M., Dunbar, S., Piepmeier, J., Yueh, S., Entekhabi, D., Cosh, M.H., Caldwell, T., Walker, J., Wu, X., Berg, A., Rowlandson, T., Pacheco, A., McNairn, H., Thibeault, M., Martínez-Fernández, J., González-Zamora, A., Seyfried, M., Bosch, D., Starks, P., Goodrich, D., Prueger, J., Palecki, M., Small, E.E., Zreda, M., Calvet, J., Crow, W.T., Kerr, Y., 2016. Assessment of the SMAP passive soil moisture product. *IEEE Trans. Geosci. Remote Sens.* 54 (8), 4994–5007.
- Chan, S., Bindlish, R., O'Neill, P., Jackson, T., Chaubell, J., Piepmeier, J., Dunbar, A., Colliander, A., Chen, F., Entekhabi, D., Yueh, S., Cosh, M., Caldwell, T., Walker, J., Wu, X., Berg, A., Rowlandson, T., Pacheco, A., McNairn, H., Thibeault, M., Martínez-Fernández, J., González-Zamora, A., Uldall, F., Seyfried, M., Bosch, D., Starks, P., Holifield Collins, C., Prueger, J., Su, Z., van der Velde, R., Asanuma, J., Palecki, M., Small, E., Zreda, M., Calvet, J.-C., Crow, W., Kerr, Y., 2017. Development and validation of the SMAP enhanced passive soil moisture product. In: *Proceedings of the 37th IEEE International Geoscience and Remote Sensing Symposium 2017*. NASA, Goddard Space Flight Center, Fort Worth, TX, United States, pp. 23–28.
- Chan, S.K., Bindlish, R., O'Neill, P., Jackson, T., Njoku, E., Dunbar, S., Chaubell, J., Piepmeier, J., Yueh, S., Entekhabi, D., Colliander, A., Chen, F., Cosh, M.H., Caldwell, T., Walker, J., Berg, A., McNairn, H., Thibeault, M., Martínez-Fernández, J., Uldall, F., Seyfried, M., Bosch, D., Starks, P., Holifield Collins, C., Prueger, J., van der Velde, R., Asanuma, J., Palecki, M., Small, E.E., Zreda, M., Calvet, J., Crow, W.T., Kerr, Y., 2018. Development and assessment of the SMAP enhanced passive soil moisture product. *Remote Sens. Environ.* 204, 931–941.
- Chaubell, J., Yueh, S., Entekhabi, D., Peng, J., 2016. Resolution enhancement of SMAP radiometer data using the Backus Gilbert optimum interpolation technique. In: *Geoscience and Remote Sensing Symposium (IGARSS), 2016 IEEE International*. IEEE, pp. 284–287.
- Chauhan, N., Miller, S., Ardanuy, P., 2003. Spaceborne soil moisture estimation at high resolution: a microwave-optical/IR synergistic approach. *Int. J. Remote Sens.* 24 (22), 4599–4622.
- Chen, M., Willgoose, G.R., Saco, P.M., 2014. Spatial prediction of temporal soil moisture dynamics using HYDRUS-1D. *Hydro. Process.* 28 (2), 171–185.
- Chen, Y., Yang, K., Qin, J., Cui, Q., Lu, H., La, Z., Han, M., Tang, W., 2017. Evaluation of SMAP, SMOS and AMSR2 soil moisture retrievals against observations from two networks on the Tibetan Plateau. *J. Geophys. Res.: Atmos.*
- Colliander, A., Jackson, T.J., Bindlish, R., Chan, S., Das, N., Kim, S.B., Cosh, M.H., Dunbar, R.S., Dang, L., Pashaian, L., Asanuma, J., Aida, K., Berg, A., Rowlandson, T., Bosch, D., Caldwell, T., Caylor, K., Goodrich, D., al Jassar, H., Lopez-Baeza, E., Martínez-Fernández, J., González-Zamora, A., Livingston, S., McNairn, H., Pacheco, A., Moghaddam, M., Montzka, C., Notarnicola, C., Niedrist, G., Pellarin, T., Prueger, J., Pulliainen, J., Rautiainen, K., Ramos, J., Seyfried, M., Starks, P., Su, Z., Zeng, Y., van der Velde, R., Thibeault, M., Dorigo, W., Vreugdenhil, M., Walker, J.P., Wu, X., Moneris, A., O'Neill, P.E., Entekhabi, D., Njoku, E.G., Yueh, S., 2017a. Validation of SMAP surface soil moisture products with core validation sites. *Remote Sens. Environ.* 191, 215–231.
- Colliander, A., Fisher, J.B., Halverson, G., Merlin, O., Misra, S., Bindlish, R., Jackson, T.J., Yueh, S., 2017b. Spatial downscaling of SMAP soil moisture using MODIS land surface temperature and NDVI during SMAPVEX15. *IEEE Geosci. Remote Sens. Lett.* 14 (11), 2107–2111.
- Colliander, A., Jackson, T.J., Chan, S.K., O'Neill, P., Bindlish, R., Cosh, M.H., Caldwell, T., Walker, J.P., Berg, A., McNairn, H., Thibeault, M., Martínez-Fernández, J., Jensen, K.H., Asanuma, J., Seyfried, M.S., Bosch, D.D., Starks, P.J., Holifield Collins, C., Prueger, J.H., Su, Z., Lopez-Baeza, E., Yueh, S.H., 2018. An assessment of the differences between spatial resolution and grid size for the SMAP enhanced soil moisture product over homogeneous sites. *Remote Sens. Environ.* 207, 65–70.
- Corbella, I., Torres, F., Duffo, N., González-Gambau, V., Pablos, M., Duran, I., Martín-Neira, M., 2011. MIRAS calibration and performance: results from the SMOS in-orbit commissioning phase. *IEEE Trans. Geosci. Remote Sens.* 49 (9), 3147–3155.
- Cosh, M.H., Jackson, T.J., Moran, S., Bindlish, R., 2008. Temporal persistence and stability of surface soil moisture in a semi-arid watershed. *Remote Sens. Environ.* 112 (2), 304–313.
- Crow, W.T., Berg, A.A., Cosh, M.H., Loew, A., Mohanty, B.P., Panciera, R., de Rosnay, P., Ryu, D., Walker, J.P., 2012. Upscaling sparse ground-based soil moisture observations for the validation of coarse-resolution satellite soil moisture products. *Rev. Geophys.* 50 (2).
- Cui, C., Xu, J., Zeng, J., Chen, K., Bai, X., Lu, H., Chen, Q., Zhao, T., 2017. Soil moisture mapping from satellites: an intercomparison of SMAP, SMOS, FY3B, AMSR2, and ESA CCI over two dense network regions at different spatial scales. *Remote Sens.* 10 (1), 33.
- Dall'Amico, J.T., Schlenz, F., Loew, A., Mauser, W., 2012. First results of SMOS soil moisture validation in the upper Danube catchment. *IEEE Trans. Geosci. Remote Sens.* 50 (5), 1507–1516.
- Das, N.N., Entekhabi, D., Njoku, E.G., 2011. An algorithm for merging SMAP radiometer and radar data for high-resolution soil-moisture retrieval. *IEEE Trans. Geosci. Remote Sens.* 49 (5), 1504–1512.
- Das, N.N., Entekhabi, D., Njoku, E.G., Shi, J.J., Johnson, J.T., Colliander, A., 2014. Tests of the SMAP combined radar and radiometer algorithm using airborne field campaign observations and simulated data. *IEEE Trans. Geosci. Remote Sens.* 52 (4), 2018–2028.
- Das, N.N., Entekhabi, D., Dunbar, R.S., Colliander, A., Chen, F., Crow, W., Jackson, T.J., Berg, A., Bosch, D.D., Caldwell, T., Cosh, M.H., Collins, C.H., Lopez-Baeza, E., Moghaddam, M., Rowlandson, T., Starks, P.J., Thibeault, M., Walker, J.P., Wu, X., O'Neill, P.E., Yueh, S., Njoku, E.G., 2018. The SMAP mission combined active-passive soil moisture product at 9 km and 3 km spatial resolutions. *Remote Sens. Environ.* 211, 204–217.
- Das, N., Dunbar, R.S., 2018. Level 2 SMAP/Sentinel Active/Passive Soil Moisture Product Specification Document, Release 2, JPL D-56548. Jet Propulsion Laboratory, CA.
- de Alcântara Silva, V.M., Gama, C.M., dos Santos, É.G., Nunes, S.H.P., dos Santos, C.A.C., 2016. Characterization NDVI space-time and surface and analysis phytosociological albedo for São João do Cariri. *J. Hyperspect. Remote Sens.* 6 (6), 305–315.
- De'ath, G., Fabricius, K.E., 2000. Classification and regression trees: a powerful yet simple technique for ecological data analysis. *Ecology* 81 (11), 3178–3192.
- Dente, L., Su, Z., Wen, J., 2012. Validation of SMOS soil moisture products over the Maqui and Twente regions. *Sensors* 12 (8), 9965–9986.
- Dickinson, R.E., Berry, J.A., Bonan, G.B., Collatz, G.J., Field, C.B., Fung, I.Y., Goulden, M., Hoffmann, W.A., Jackson, R.B., Myneni, R., Sellers, P.J., Shaikh, M., 2002. Nitrogen controls on climate model evapotranspiration. *J. Clim.* 15 (3), 278–295.
- Didan, K., 2015. MYD13A2 MODIS/aqua vegetation indices 16-day L3 global 1km SIN GRID V006. NASA EOSDIS Land Processes DAAC. <https://doi.org/10.5067/modis/myd13a2.006>.
- Dirmeyer, P.A., Wu, J., Norton, H.E., Dorigo, W.A., Quiring, S.M., Ford, T.W., Santanello Jr, J.A., Bosilovich, M.G., Ek, M.B., Koster, R.D., Balsamo, G., Lawrence, D.M., 2016. Confronting weather and climate models with observational data from soil moisture networks over the United States. *J. Hydrometeorol.* 17 (4), 1049–1067.
- Djamai, N., Magagi, R., Goita, K., Hosseini, M., Cosh, M.H., Berg, A., Toth, B., 2015. Evaluation of SMOS soil moisture products over the CanEx-SM10 area. *J. Hydrol.* 520, 254–267.
- Djamai, N., Magagi, R., Goita, K., Merlin, O., Kerr, Y., Roy, A., 2016. A combination of DISPATCH downscaling algorithm with CLASS land surface scheme for soil moisture estimation at fine scale during cloudy days. *Remote Sens. Environ.* 184, 1–14.
- Engman, E.T., 1991. Applications of microwave remote sensing of soil moisture for water resources and agriculture. *Remote Sens. Environ.* 35 (2–3), 213–226.
- Entekhabi, D., Njoku, E.G., O'Neill, P.E., Kellogg, K.H., Crow, W.T., Edelstein, W.N., Entin, J.K., Goodman, S.D., Jackson, T.J., Johnson, J., Kimball, J., Piepmeier, J.R., Koster, R.D., Martin, N., McDonald, K.C., Moghaddam, M., Moran, S., Reichle, R., Shi, J.C., Spencer, M.W., Thurman, S.W., Tsang, L., Van Zyl, J., 2010a. The soil moisture active passive (SMAP) mission. *Proc. IEEE* 98 (5), 704–716.
- Entekhabi, D., Reichle, R.H., Koster, R.D., Crow, W.T., 2010b. Performance metrics for soil moisture retrievals and application requirements. *J. Hydrometeorol.* 11 (3), 832–840.
- Entekhabi, D., Yueh, S., O'Neill, P.E., Kellogg, K.H., Allen, A., Bindlish, R., Brown, M., Chan, S., Colliander, A., Crow, W.T., Das, N., De Lannoy, G., Dunbar, R.S., Edelstein, W.N., Entin, J.K., Escobar, V., Goodman, S.D., Jackson, T.J., Jai, B., Johnson, J., Kim, E., Kim, S., Kimball, J., Koster, R.D., Leon, A., McDonald, K.C., Moghaddam, M., Mohammed, P., Moran, S., Njoku, E.G., Piepmeier, J.R., Reichle, R., Rogez, F., Shi, J.C., Spencer, M.W., Thurman, S.W., Tsang, L., Van Zyl, J., Weiss, B., West, R., 2014. *SMAP Handbook-Soil Moisture Active Passive: Mapping Soil Moisture and Freeze/Thaw From Space*, JPL Publication JPL 400–1567. Jet Propulsion Laboratory, Pasadena, California.
- Famiglietti, J.S., Ryu, D., Berg, A.A., Rodell, M., Jackson, T.J., 2008. Field observations of soil moisture variability across scales. *Water Resour. Res.* 44 (1).
- Fang, B., Lakshmi, V., Bindlish, R., Jackson, T.J., Cosh, M., Basara, J., 2013. Passive microwave soil moisture downscaling using vegetation index and skin surface temperature. *Vadose Zone J.* 12 (3).

- Fang, B., Lakshmi, V., 2014. Soil moisture at watershed scale: Remote sensing techniques. *J. Hydrol.* 516, 258–272.
- Fang, B., Lakshmi, V., Bindlish, R., Jackson, T., 2018. Downscaling of SMAP soil moisture using land surface temperature and vegetation data. *Vadose Zone J.* 17 (1).
- Farrar, T., Nicholson, S., Lare, A., 1994. The influence of soil type on the relationships between NDVI, rainfall, and soil moisture in semiarid Botswana. II. NDVI response to soil moisture. *Remote Sens. Environ.* 50 (2), 121–133.
- Gao, Y., Walker, J.P., Ye, N., Panciera, R., Moneris, A., Ryu, D., Rüdiger, C., Jackson, T.J., 2018. Evaluation of the Tau-Omega model for passive microwave soil moisture retrieval using SMAPEX datasets. *IEEE J. Sel. Top. Appl. Earth Obs. Remote Sens.* 11 (3), 888–895.
- Gherboudj, I., Magagi, R., Goita, K., Berg, A.A., Toth, B., Walker, A., 2012. Validation of SMOS data over agricultural and boreal forest areas in Canada. *IEEE Trans. Geosci. Remote Sens.* 50 (5), 1623–1635.
- Gómez-Plaza, A., Alvarez-Rogel, J., Albaladejo, J., Castillo, V., 2000. Spatial patterns and temporal stability of soil moisture across a range of scales in a semi-arid environment. *Hydrol. Process.* 14 (7), 1261–1277.
- Grayson, R.B., Western, A.W., 1998. Towards areal estimation of soil water content from point measurements: time and space stability of mean response. *J. Hydrol.* 207 (1–2), 68–82.
- Grundy, M.J., Rossel, R.A.V., Searle, R.D., Wilson, P.L., Chen, C., Gregory, L.J., 2015. Soil and landscape grid of Australia. *Soil Res.* 53 (8), 835–844.
- Hanson, B., Orloff, S., Peters, D., 2000. Monitoring soil moisture helps refine irrigation management. *Calif. Agric.* 54 (3), 38–42.
- Huszar, T., Mika, J., Loczy, D., Molnar, K., Kertesz, A., 1999. Climate change and soil moisture: a case study. *Phys. Chem. Earth Part A.* 24 (10), 905–912.
- Jackson, T.J., Bindlish, R., Cosh, M.H., Zhao, T., Starks, P.J., Bosch, D.D., Seyfried, M., Moran, M.S., Goodrich, D.C., Kerr, Y.H., Leroux, D., 2012. Validation of Soil Moisture and Ocean Salinity (SMOS) soil moisture over watershed networks in the US. *IEEE Trans. Geosci. Remote Sens.* 50 (5), 1530–1543.
- Jackson, T.J., Colliander, A., Kimball, J., Reichle, R., Derksen, C., Crow, W., Entekhabi, D., O'Neill, P., Njoku, E., 2014. SMAP Science Data Calibration and Validation Plan (Revision A), Soil Moisture Active Passive (SMAP) Mission Science Document. JPL D-52544. Jet Propulsion Laboratory, Pasadena, CA.
- Karthikeyan, L., Pan, M., Wanders, N., Kumar, D.N., Wood, E.F., 2017a. Four decades of microwave satellite soil moisture observations: Part 1. A review of retrieval algorithms. *Adv. Water Resour.* 109, 106–120.
- Karthikeyan, L., Pan, M., Wanders, N., Kumar, D.N., Wood, E.F., 2017b. Four Decades of microwave satellite soil moisture observations: Part 2. Product validation and inter-satellite comparisons. *Adv. Water Resour.* 109, 236–252.
- Kerr, Y.H., Waldteufel, P., Wigneron, J., Delwart, S., Cabot, F., Boutin, J., Escorihuela, M., Font, J., Reul, N., Gruhier, C., 2010. The SMOS mission: new tool for monitoring key elements of the global water cycle. *Proc. IEEE* 98 (5), 666–687.
- Kerr, Y.H., Waldteufel, P., Richaume, P., Wigneron, J.P., Ferrazzoli, P., Mahmoodi, A., Al Bitar, A., Cabot, F., Gruhier, C., Juglea, S.E., Leroux, D., Mialon, A., Delwart, S., 2012. The SMOS soil moisture retrieval algorithm. *IEEE Trans. Geosci. Remote Sens.* 50 (5), 1384–1403.
- Kerr, Y.H., Jacquette, E., Al Bitar, A., Cabot, F., Mialon, A., Richaume, P., Quesney, A., Berthon, L., 2013. CATDS SMOS L3 soil moisture retrieval processor Algorithm Theoretical Baseline Document (ATBD), Technical Note SO-TN-CBSA-GS-0029, Issue 2.0. CESBIO, Toulouse, France.
- Kerr, Y.H., Wigneron, J.P., Al Bitar, A., Mialon, A., Srivastava, P.K., 2016. Soil Moisture from Space: Techniques and Limitations. In: Srivastava, P.K., Petropoulos, G.P., Kerr, Y.H. (Eds.), *Satellite Soil Moisture Retrieval: Techniques and Applications*. Elsevier Inc., Amsterdam, The Netherlands, pp. 3–27.
- Kunkel, V., Wells, T., Hancock, G., 2016. Soil temperature dynamics at the catchment scale. *Geoderma* 273, 32–44.
- Lacava, T., Cuomo, V., Di Leo, E.V., Pergola, N., Romano, F., Tramutoli, V., 2005. Improving soil wetness variations monitoring from passive microwave satellite data: the case of April 2000 Hungary flood. *Remote Sens. Environ.* 96 (2), 135–148.
- Leroux, D.J., Das, N.N., Entekhabi, D., Colliander, A., Njoku, E., Jackson, T.J., Yueh, S., 2016. Active-passive soil moisture retrievals during the SMAP validation experiment 2012. *IEEE Geosci. Remote Sens. Lett.* 13 (4), 475–479.
- Lorenz, D.J., Otkin, J.A., Svoboda, M., Hain, C.R., Anderson, M.C., Zhong, Y., 2017. Predicting US drought monitor states using precipitation, soil moisture, and evapotranspiration anomalies. Part I: development of a nondiscrete USDM index. *J. Hydrometeorol.* 18 (7), 1943–1962.
- Martinez, C., Hancock, G., Kalma, J., Wells, T., 2007. Spatio-temporal distribution of near-surface and root zone soil moisture at the catchment scale. *Hydrol. Process.* 22 (14), 2699–2714.
- Merlin, O., Walker, J.P., Chehbouni, A., Kerr, Y., 2008. Towards deterministic downscaling of SMOS soil moisture using MODIS derived soil evaporative efficiency. *Remote Sens. Environ.* 112 (10), 3935–3946.
- Merlin, O., Duchemin, B., Hagolle, O., Jacob, F., Coudert, B., Chehbouni, G., Dedieu, G., Garatua, J., Kerr, Y., 2010. Disaggregation of MODIS surface temperature over an agricultural area using a time series of Formosat-2 images. *Remote Sens. Environ.* 114 (11), 2500–2512.
- Merlin, O., Rüdiger, C., Al Bitar, A., Richaume, P., Walker, J.P., Kerr, Y.H., 2012. Disaggregation of SMOS soil moisture in Southeastern Australia. *IEEE Trans. Geosci. Remote Sens.* 50 (5), 1556–1571.
- Mills, G.A., Webb, R., Davidson, N.E., Kepert, J., Seed, A., Abbs, D., 2010. The Pasha Bulker east coast low of 8 June 2007. CAWCR Technical Report No. 023. Centre for Australian Weather and Climate Research, Melbourne, Australia.
- Neeck, S.P., 2015. The NASA earth science flight program: An update. In: *Proceedings of SPIE 9639, Sensors, Systems, and Next-Generation Satellites XIX 2015*. Toulouse, France, 963907.
- Niclos, R., Rivas, R., García-Santos, V., Doña, C., Valor, E., Holzman, M., Bayala, M., Carmona, F., Ocampo, D., Soldano, Á., Thibeault, M., Caselles, V., Sánchez, J.M., 2016. SMOS level-2 soil moisture product evaluation in rain-fed croplands of the Pampean region of Argentina. *IEEE Trans. Geosci. Remote Sens.* 54 (1), 499–512.
- Norbriato, D., Borgia, M., Degli Esposti, S., Gaume, E., Anquetin, S., 2008. Flash flood warning based on rainfall thresholds and soil moisture conditions: An assessment for gauged and ungauged basins. *J. Hydrol.* 362 (3), 274–290.
- O'Neill, P. E., Chan, S., Njoku, E.G., Jackson, T., Bindlish, R., 2016. SMAP Enhanced L3 Radiometer Global Daily 9 km EASE-Grid Soil Moisture, Version 1. NASA National Snow and Ice Data Center Distributed Active Archive Center, Boulder, Colorado USA. doi: <https://doi.org/10.5067/ZRO7EXJ803XI>. [Accessed June 28, 2017].
- Orth, R., Seneviratne, S.I., 2014. Using soil moisture forecasts for sub-seasonal summer temperature predictions in Europe. *Clim. Dyn.* 43 (12), 3403–3418.
- Oyoshi, K., Akatsuka, S., Takeuchi, W., Sobue, S., 2014. Hourly LST monitoring with Japanese geostationary satellite MTSAT-1R over the Asia-Pacific region. *Asian J. Geoinform.* 14 (3).
- Pablos, M., Martínez-Fernández, J., Sánchez, N., González-Zamora, Á., 2017. Temporal and spatial comparison of agricultural drought indices from moderate resolution satellite soil moisture data over northwest Spain. *Remote Sens.* 9 (11).
- Pacheco, A., McNairn, H., Mahmoodi, A., Champagne, C., Kerr, Y.H., 2015. The impact of national land cover and soils data on SMOS soil moisture retrieval over Canadian agricultural landscapes. *IEEE J. Sel. Top. Appl. Earth Obs. Remote Sens.* 8 (11), 5281–5293.
- Panciera, R., Walker, J.P., Kalma, J.D., Kim, E.J., Hacker, J.M., Merlin, O., Berger, M., Skou, N., 2008. The NAFE/05/CoSMOS data set: toward SMOS soil moisture retrieval, downscaling, and assimilation. *IEEE Trans. Geosci. Remote Sens.* 46 (3), 736–745.
- Panciera, R., Walker, J.P., Kalma, J.D., Kim, E.J., Saleh, K., Wigneron, J., 2009. Evaluation of the SMOS L-MEB passive microwave soil moisture retrieval algorithm. *Remote Sens. Environ.* 113 (2), 435–444.
- Peng, J., Loew, A., Merlin, O., Verhoest, N.E., 2017. A review of spatial downscaling of satellite remotely-sensed soil moisture. *Rev. Geophys.* 55 (2), 341–366.
- Petropoulos, G., Carlson, T., Wooster, M., Islam, S., 2009. A review of Ts/Vi remote sensing based methods for the retrieval of land surface energy fluxes and soil surface moisture. *Prog. Phys. Geogr.* 33 (2), 224–250.
- Piepmeyer, J.R., Focardi, P., Horgan, K.A., Knuble, J., Ehsan, N., Lucey, J., Brambora, C., Brown, P.R., Hoffman, P.J., French, R.T., Mikhaylov, R.L., Kwack, E.-Y., Slimko, E.M., Dawson, D.A., Hudson, D., Peng, J., Mohammed, P.N., De Amici, G., Freedman, A.P., Medeiros, J., Sacks, F., Estep, R., Spencer, M.W., Cehn, C.W., Wheeler, K.B., Edelstein, W.N., O'Neill, P.E., Njoku, E.J., 2017. SMAP L-band microwave radiometer: Instrument design and first year on orbit. *IEEE Trans. Geosci. Remote Sens.* 55 (4), 1954–1966.
- Piles, M., Entekhabi, D., Camps, A., 2009. A change detection algorithm for retrieving high-resolution soil moisture from SMAP radar and radiometer observations. *IEEE Trans. Geosci. Remote Sens.* 47 (12), 4125–4131.
- Piles, M., Camps, A., Vall-Llossera, M., Corbella, I., Panciera, R., Rüdiger, C., Kerr, Y.H., Walker, J., 2011. Downscaling SMOS-derived soil moisture using MODIS visible/infrared data. *IEEE Trans. Geosci. Remote Sens.* 49 (9), 3156–3166.
- Piles, M., Sánchez, N., Vall-Llossera, M., Camps, A., Martínez-Fernández, J., Martínez, J., González-Gambau, V., 2014. A downscaling approach for SMOS land observations: evaluation of high-resolution soil moisture maps over the Iberian Peninsula. *IEEE J. Sel. Top. Appl. Earth Obs. Remote Sens.* 7 (9), 3845–3857.
- Piles, M., Petropoulos, G.P., Sánchez, N., González-Zamora, Á., Ireland, G., 2016. Towards improved spatio-temporal resolution soil moisture retrievals from the synergy of SMOS and MSG SEVIRI spaceborne observations. *Remote Sens. Environ.* 180, 403–417.
- Poe, G.A., 1990. Optimum interpolation of imaging microwave radiometer data. *IEEE Trans. Geosci. Remote Sens.* 28 (5), 800–810.
- Porporato, A., Rodriguez-Iturbe, I., 2002. Ecohydrology—a challenging multidisciplinary research perspective/Ecohydrologie: une perspective stimulante de recherche multidisciplinaire. *Hydrol. Sci. J.* 47 (5), 811–821.
- Portal, G., Vall-Llossera, M., Piles, M., Camps, A., Chaparro, D., Pablos, M., Rossato, L., 2018. A spatially consistent downscaling approach for SMOS using an adaptive moving window. *IEEE J. Selected Top. Appl. Earth Observ. Remote Sens.* 11 (6), 1883–1894.
- Rossel, R.A.V., Chen, C., Grundy, M.J., Searle, R., Clifford, D., Campbell, P.H., 2015. The Australian three-dimensional soil grid: Australia's contribution to the GlobalSoilMap project. *Soil Res.* 53 (8), 845–864.
- Rüdiger, C., Davidson, R., Hemakumara, H., Walker, J., Kalma, J., Willgoose, G., Houser, P., 2003. Catchment monitoring for scaling and assimilation of soil moisture and streamflow. In: *Proceedings of the International Congress on Modelling and Simulation (MODSIM03)*, Townsville, Australia, pp. 386–391.
- Rüdiger, C., Hancock, G., Hemakumara, H.M., Jacobs, B., Kalma, J.D., Martinez, C., Thyer, M., Walker, J.P., Wells, T., Willgoose, G.R., 2007. Goulburn River experimental catchment data set. *Water Resour. Res.* 43 (10).
- Rüdiger, C., Walker, J., Kalma, J., Willgoose, G., Houser, P., 2005. Root zone soil moisture retrieval using streamflow and surface moisture data assimilation in nested catchments. In: *MODSIM05: International Congress on Modelling and Simulation*, Melbourne, pp. 1458–1464.
- Sabaghy, S., Walker, J.P., Renzullo, L.J., Jackson, T.J., 2018. Spatially enhanced passive microwave derived soil moisture: capabilities and opportunities. *Remote Sens. Environ.* 209, 551–580.
- Sánchez-Ruiz, S., Piles, M., Sánchez, N., Martínez-Fernández, J., Vall-Llossera, M., Camps, A., 2014. Combining SMOS with visible and near/shortwave/thermal infrared satellite data for high resolution soil moisture estimates. *J. Hydrol.* 516, 273–283.
- Sandholt, I., Rasmussen, K., Andersen, J., 2002. A simple interpretation of the surface temperature/vegetation index space for assessment of surface moisture status.

- Remote Sens. Environ. 79 (2–3), 213–224.
- Schmugge, T., 1976. Remote Sensing of Soil Moisture. Goddard Space Flight Center, USA.
- Schmugge, T., Jackson, T., 1993. Passive microwave remote sensing of soil moisture. *EARSeL Adv. Remote Sens.* 2 (2), 5–14.
- Schmugge, T., O'Neill, P.E., Wang, J.R., 1986. Passive microwave soil moisture research. *IEEE Trans. Geosci. Remote Sens.* GE-24 (1), 12–22.
- Sellers, W.D., 1965. *Physical Climatology*. University of Chicago Press, Chicago, Illinois, United States.
- Senanayake, I.P., Yeo, I.Y., Tangdamrongsub, N., Willgoose, G.R., Hancock, G.R., Wells, T., 2017. Disaggregation of SMAP radiometric soil moisture measurements at catchment scale using MODIS land surface temperature data. In: *Proceedings of the 4th Annual Conference of Research@Locate*, Sydney, pp. 19–24.
- Tramblay, Y., Bouvier, C., Martin, C., Didon-Lescot, J., Todorovik, D., Domergue, J., 2010. Assessment of initial soil moisture conditions for event-based rainfall-runoff modelling. *J. Hydrol.* 387 (3), 176–187.
- Tucker, C.J., 1979. Red and photographic infrared linear combinations for monitoring vegetation. *Remote Sens. Environ.* 8 (2), 127–150.
- Ulaby, F., Moore, R., Fung, A., 1986. *Microwave remote sensing: Active and passive. Volume 3, From theory to applications*. Artech House, Norwood, MA.
- Van Dijk, A.I.J.M., Beck, H.E., Crosbie, R.S., Jeu, R.A.M., Liu, Y.Y., Podger, G.M., Timbal, B., Viney, N.R., 2013. The Millennium Drought in southeast Australia (2001–2009): Natural and human causes and implications for water resources, ecosystems, economy, and society. *Water Resour. Res.* 49 (2), 1040–1057.
- Vanderlinden, K., Vereecken, H., Hardelauf, H., Herbst, M., Martínez, G., Cosh, M.H., Pachepsky, Y.A., 2012. Temporal stability of soil water contents: a review of data and analyses. *Vadose Zone J.* 11 (4).
- Verstraeten, W.W., Veroustraete, F., van der Sande, C.J., Grootaers, I., Feyen, J., 2006. Soil moisture retrieval using thermal inertia, determined with visible and thermal spaceborne data, validated for European forests. *Remote Sens. Environ.* 101 (3), 299–314.
- Wan, Z., 2008. New refinements and validation of the MODIS land-surface temperature/emissivity products. *Remote Sens. Environ.* 112 (1), 59–74.
- Wan, Z., Hook, S., Hulley, G., 2015. MYD11A1 MODIS/aqua land surface temperature/emissivity daily L3 global 1km SIN grid V006. NASA EOSDIS Land Processes DAAC. <https://doi.org/10.5067/modis/myd11a1.006>.
- Wang, A., Lettenmaier, D.P., Sheffield, J., 2011. Soil moisture drought in China, 1950–2006. *J. Clim.* 24 (13), 3257–3271.
- Wang, J., Bras, R., Sivandran, G., Knox, R., 2010. A simple method for the estimation of thermal inertia. *Geophys. Res. Lett.* 37 (5).
- Wigneron, J.-P., Kerr, Y., Waldteufel, P., Saleh, K., Escorihuela, M.-J., Richaume, P., Ferrazzoli, P., de Rosnay, P., Gurney, R., Calvet, J.-C., Grant, J.P., Guglielmetti, M., Hornbuckle, B., Mätzler, C., Pellarin, T., Schwank, M., 2007. L-band microwave emission of the biosphere (L-MEB) model: description and calibration against experimental data sets over crop fields. *Remote Sens. Environ.* 107 (4), 639–655.
- Wu, X., Walker, J.P., Rüdiger, C., Panciera, R., Gao, Y., 2017. Medium-resolution soil moisture retrieval using the bayesian merging method. *IEEE Trans. Geosci. Remote Sens.* 55 (11), 6482–6493.
- Yamamoto, Y., Ishikawa, H., 2018. Thermal land surface emissivity for retrieving land surface temperature from Himawari-8. *J. Meteorol. Soc. Jpn. Ser. II* 96, 43–58.